Check for updates

Hydrological Processes

WILEY

RESEARCH ARTICLE

Mapping and Modelling Specific Sediment Yield and Future Soil Erosion Trends in the Jhelum Catchment, India

Shahid Ul Islam[1,2] | Ravi Raj[3] | Epari Ritesh Patro[4] | Manabendra Saharia[1,5] | Sumedha Chakma[1]

[1]Department of Civil Engineering, Indian Institute of Technology (IIT) Delhi, New Delhi, India | [2]Department of Civil Engineering, Baba Ghulam Shah Badshah University, Rajouri, Jammu and Kashmir, India | [3]United States Department of Agriculture (USDA), Agricultural Research Service, Maricopa, Arizona, USA | [4]Water, Energy and Environmental Engineering Research Unit, Faculty of Technology, University of Oulu, Oulu, Finland | [5]Yardi School of Artificial Intelligence, Indian Institute of Technology Delhi, New Delhi, India

Correspondence: Shahid Ul Islam (shahid.ul.islam@civil.iitd.ac.in)

Received: 30 December 2024 | **Revised:** 14 May 2025 | **Accepted:** 1 September 2025

Funding: This work was supported by Jammu and Kashmir Science, Technology & Innovation Council (JKST&IC), Union Territory of Jammu and Kashmir (UT of J&K), which holds no responsibility for the conclusions drawn.

Keywords: climate modelling | Jhelum catchment | land use | RUSLE | sediment yield | soil erosion

ABSTRACT

Soil erosion management is a crucial component of sustainable soil and water management, especially in regions where agricultural productivity is at risk and areas that are more vulnerable to the impacts of climate change, such as the Himalayan region. This study explores soil erosion dynamics in the Jhelum Catchment, India, using advanced mapping and modelling techniques to analyse and predict trends of potential soil loss from 2020 to 2090. The study integrates the RUSLE model with projected climate to assess the impact of climate change on soil erosion and rainfall erosivity. The InVEST SDR model is used to quantify sediment transport and specific sediment yield, enhancing our understanding of the hydrological processes that drive soil erosion and sediment mobilisation in the Jhelum Catchment. The RUSLE, along with advanced climate modelling, land-use data, and spatial analysis, is used in this study to predict trends in soil erosion. Climate data from the Coupled Model Intercomparison Project Phase 6 (CMIP6) is combined with data from the India Meteorological Department (IMD) to project rainfall erosivity (R). R, along with soil erodibility (K), slope length and steepness (LS), land cover (C), and support practices (P) factors, are mapped and applied in the Revised Universal Soil Loss Equation (RUSLE) model, which evaluates the potential for soil erosion. This study forecasts soil loss trends by combining climate data, land-use information, and spatial analysis from 2020 to 2090 under two scenarios [SSP245 (moderate emissions) and SSP585 (high emissions)]. Results indicate escalating soil loss, particularly in less severe areas in 2020, highlighting the dynamic threat. The mean value of soil loss for SSP245 exhibits a continuous rise from 46.17 t/ha/year in 2030 to 51.54 t/ha/year in 2090. SSP585 shows a more severe trend, peaking at 71.67 t/ha/year in 2090. The study also classifies potential soil loss into severity classes, observing a decrease in the percentage area of less severe classes over time. Soil erosion class-wise projections from 2020 to 2090, based on LULC and soil type, reveal trends across various categories of land use, including Agriculture, Forest, Built-up Areas, and Grass/Grazing Land, as well as soil types like Cambisols, Lithosols, Glaciers, and Inland Water. These results highlight the urgent need for proactive interventions, offering practical insights for sustainable land management and providing actionable guidance for strategic planning and policy development focused on sustainable agricultural practices and climate change adaptation. This novel approach integrates advanced modelling and GIS-based analysis, making it applicable to other catchments with similar climate and land-use challenges. The study's findings directly apply to informing land management strategies, making the research highly relevant and practical.

© 2025 John Wiley & Sons Ltd.

1 | Introduction

The significant effects of human activities on the depletion of natural resources have become increasingly clear (Lampert 2019). To tackle this issue, it is essential to use effective tools such as Geographic Information Systems (GIS) and hydrological models. These tools are crucial for evaluating the consequences of human activities (Berger et al. 2021) and for understanding changes in hydrology (Genxu et al. 2005). Climate change influences water availability in the Heihe River Basin catchment (Zhang et al. 2016) and enhances hydrological components, altering their patterns and regimes (Stagl et al. 2014). Climate change and urban expansion are increasing flood risks in the Ganges-Brahmaputra-Meghna (GBM) delta (Wu et al. 2024). The frequency of extreme weather events is expected to increase significantly due to climate change (Solomon 2007). Furthermore, an increase in precipitation intensity leads to greater erosion and higher sediment yield (Tao et al. 2017). Urgent action is required to mitigate the impacts of climate change on water availability (Tabari 2020). Changes in land use have a significant impact on hydrological processes and sediment yield (Sharma et al. 2023; Siswanto and Francés 2019). Alterations in land use significantly influence soil erosion rates, especially in areas undergoing rapid development (Li et al. 2014). Extensive research highlights a crucial link between climate change and sediment yield, underscoring the importance of addressing this pressing issue (Chuenchum et al. 2020). Projections indicate climate-induced alterations will likely impact sediment yields (Aghsaei et al. 2020). Climate change influences precipitation patterns, which in turn affect the water cycle (Kalantari et al. 2014). Increased temperatures, more significant snowmelt, and higher precipitation have increased watershed sediment yield (Stryker et al. 2018). Temperature-based hotspots are crucial for assessing climate change impacts and regional adaptation strategies (Sarkar and Maity 2024). With alluvial rivers, the sub-Himalayan region presents challenges like landslides and floods from heavy rainfall (Dhakal 2015). Sediments in rivers complicate infrastructure design and maintenance (Kothyari 2009). Understanding the origins of sediment is vital for accurately assessing soil erosion rates (Kothyari et al. 2002). Analysing sediment yield is imperative, as its deposition directly affects reservoir capacity, increases floodplain size, and influences water resources (Dutta 2016). Gholami et al. (2020) demonstrated the effective use of self-organising maps (SOM) with GIS for soil erosion mapping. Climate change influences the movement of sediments and the water resources availability (DeFries and Eshleman 2004). Techniques for modelling sediment transport, including sediment transport equations, artificial neural networks, and statistical methods, are employed to predict sediment movement in watersheds (Asheghi and Hosseini 2020; Avand et al. 2023). Machine learning techniques are being applied to predict soil erosion by assessing various factors, including rainfall, types of land cover, and human influences (Hou et al. 2024). Zeghmar et al. (2024) employed machine learning to improve RUSLE-based soil erosion modelling in Algeria. Rainfall erosivity (R) is essential for estimating soil erosion (Williams 1975). Research efforts, like the global erosivity map (Panagos et al. 2017), high-resolution R factor maps (Raj et al. 2022), and soil erodibility maps (Raj et al. 2023), contribute to understanding erosion trends. Raj et al. (2024) conducted the first extensive mapping of soil erosion across India, demonstrating an average potential soil loss of 21 tons per hectare each year (Raj et al. 2024). Projections of future erosivity trends aid in managing soil erosion and water resources, showcasing the relevance of climate-induced environmental transformations (Panagos et al. 2022). By 2100, global soil erosion and sediment transport could increase by over 10% due to changing land use practices. This highlights the necessity of implementing sustainable land management practices to address this problem (Borrelli et al. 2017). The Jhelum catchment in India is highly susceptible to erosion due to its distinct topography; however, limited studies have been conducted in this crucial area. Existing research has predominantly focused on sediment lithology, which emphasises the critical need for a comprehensive study on soil erosion in this data-scarce region. Addressing this gap is essential for advancing our understanding and effective management of soil erosion issues. The Jhelum Basin in Kashmir has been chosen for investigation due to its significant agricultural productivity, diverse topography, and soil erosion and flooding vulnerability. Limited studies have examined the combined impact of land use and climate change on hydrology and sediment yield in this region. Given its substantial glacial resources and vulnerability to climate change, the Jhelum Basin provides a crucial setting to analyse future soil erosion trends and sediment management challenges under changing climatic conditions. These factors provide an opportunity to understand erosion dynamics under varying climatic conditions better. LULC changes in the Upper Jhelum Basin have significantly altered flow regimes and runoff coefficients, increased low-flow durations, and affected water availability (Islam and Chakma 2024a). CMIP6 climate data and the RUSLE model are utilised to analyse the effects of climate change on soil erosion. To advance the understanding of hydrological processes under changing climate and land use conditions, this study investigates the evolving soil erosion dynamics in the Jhelum Catchment, a climate-sensitive region of the western Himalayas. This study addresses three research questions: (1) How will projected climate changes (SSP245 and SSP585) from 2020 to 2090 affect soil erosion in the Jhelum Catchment? (2) What are the spatial and temporal patterns of soil erosion severity across different land use/land cover types and soil categories? (3) How do rainfall erosivity trends, derived from CMIP6 and IMD datasets, influence sediment transport and soil degradation under future scenarios? To answer these, the study aims to: (i) estimate baseline specific sediment yield using RUSLE and InVEST SDR models, (ii) evaluate the impacts of projected climate scenarios on soil erosion rates, and (iii) identify high-risk erosion zones and vulnerable LULC and soil types for climate-resilient land management. This approach enhances understanding of climate-driven hydrological changes, offering practical insights for sustainable land and watershed management. The novelty of this study lies in integrating RUSLE with advanced climate modelling and GIS-based spatial analysis to assess long-term soil erosion trends under SSP scenarios. Unlike previous studies, it evaluates the combined impact of climate change on erosion, offering crucial insights for sustainable land management. This study could offer valuable insights that can be effectively applied to other areas confronting similar soil erosion challenges.

10991085, 2025, 9, Downloaded from https://onlinelibrary.wiley.com/doi/10.1002/hyp.70262 by INDIAN INSTITUTE OF TECHNOLOGY (NON -EAL), Wiley Online Library on [21/09/2025]. See the Terms and Conditions (https://onlinelibrary.wiley.com/terms-and-conditions) on Wiley Online Library for rules of use; OA articles are governed by the applicable Creative Commons License

2 | Materials and Methods

2.1 | Study Area Description and Characteristics

The Jhelum River originates from the Verinag in the Kashmir Valley, India, and is an important Indus River tributary. Its watershed encompasses 24 catchment areas. The left-bank catchments are sourced from the Pir Panjal range, while the right-bank areas are derived from the Great Himalayan Mountains (Romshoo et al. 2018). The Jhelum Basin, renowned for its diverse topography, is a crucial river basin that supports irrigation, hydropower, and various human activities, with its water primarily sourced from the Pir Panjal range (Khanday et al. 2021). The watershed features a varied landscape, including medium to high hills, mountain ranges, and alluvial channels (Bhat, Alam, Ahmad, Kotlia, et al. 2019). The region mainly consists of silt loam and clay loam soils. Winter is the season with the most rainfall, influenced by western disturbances. During spring, the northern slopes of the Pir Panjal range experience the highest levels of rainfall, significantly impacting soil erosion (Bhutiyani et al. 2007; Romshoo et al. 2018).

The Jhelum River runs through the Kashmir Valley's alluvial plain, fed by streams from the surrounding mountains. The area's geographical and climatic features make it prone to natural hazards, particularly flooding and soil erosion in the Jhelum River's upper reaches, leading to sediment accumulation in the Wular Lake (Ganaie et al. 2018). The watershed experiences weathering as a result of its harsh climatic conditions, deforestation, regional development, seismic activity, and heavy rainfall, all of which contribute to increased sedimentation (Romshoo et al. 2018). Recent demographic studies indicate a population increase and a shift from agriculture to horticulture, driven by evolving economic opportunities (Romshoo and Rashid 2014). The complex landscape of the area and limited data hinder the assessment of extreme floods and their interactions with the land surface (Romshoo et al. 2012). The climate-induced changes in the upper Jhelum River led to increased floods and soil erosion, impacting Wular Lake's size and depth (Bhat, Alam, Ahmad, et al. 2019; Ganaie et al. 2018). The Jhelum River is a significant sediment source for Wular Lake, emphasising the importance of understanding its hydrological dynamics and sediment transport processes (Meraj et al. 2018). Sediment mobilisation is influenced by factors like deforestation, regional development, and floods (Bhatt et al. 2017; Romshoo and Rashid 2014). Population growth, agricultural shifts to horticulture, challenging terrain, and data limitations compound challenges in the Jhelum Basin, while climate variability intensifies flood frequency (Romshoo et al. 2012, 2018). Flood events in the Jhelum River have increased due to climate change (Bhat, Alam, Ahmad, et al. 2019). Additionally, steep slopes in the upper reaches cause significant soil erosion, leading to Wular Lake's shrinking size, reduced depth, and increased aquatic plant growth (Ganaie et al. 2018). Population-driven land-use changes have impacted the upper Jhelum Basin's hydrological flow patterns and runoff coefficients. This has increased low flood frequency and altered flow duration curves, demonstrating the need to integrate land-use considerations into water management and infrastructure design (Islam and Chakma 2024a). Recent studies indicate a significant rise in rainfall erosivity in the Jhelum Catchment due to climate change, with projections showing an increase in *R* values from 2020 to 2090, highlighting the urgent need for mitigation measures (Islam and Chakma 2024b). Given the risk of flooding, taking proactive measures and developing infrastructure carefully is essential (Bhat, Alam, Ahmad, Farooq, and Ahmad 2019). Figure 1A shows the geographical location of the study area. The soil map in Figure 1B, created using the FAO-UNESCO Soil Map, identifies four soil classes: Cambisols with horizon differentiation, Lithosols characterised by noticeable unweathered rock fragments, Inland Water areas, and Glaciers. Each of these classes influences the local landscape and land use differently. The valley region is mainly covered with Cambisols, while the mountainous region is covered with Lithosols, as depicted from the soil class map.

2.2 | Data Sources

Soil erosion and sediment yield in the Jhelum Catchment area are assessed using the RUSLE model which takes into consideration precipitation, soil characteristics, landscape features,

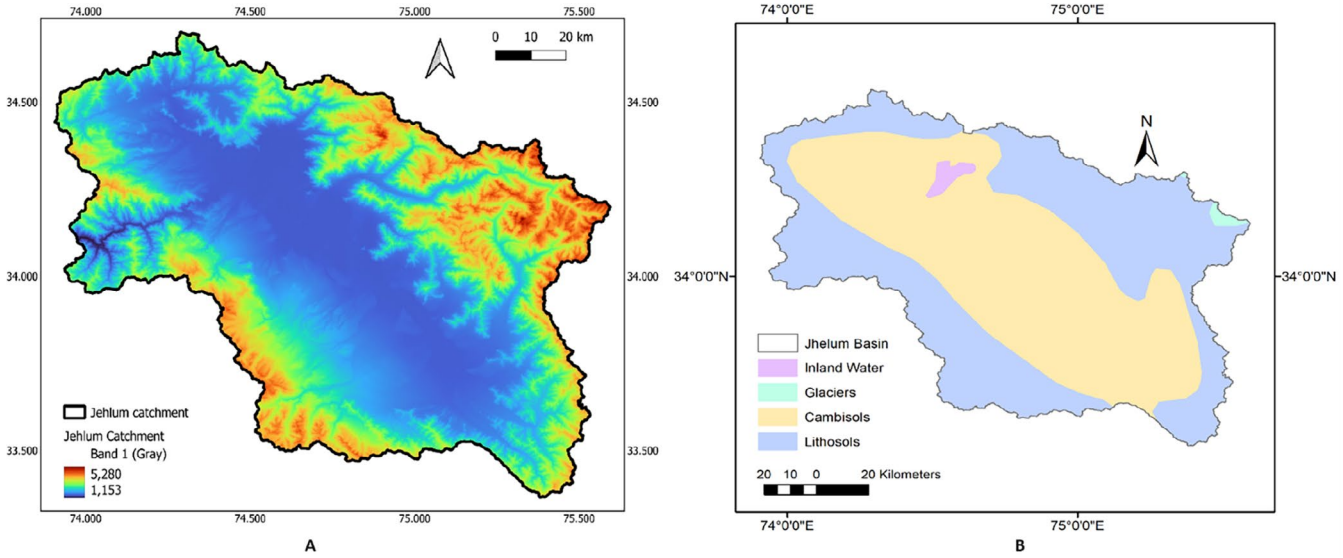

FIGURE 1 | (A) Location of the Jhelum Catchment and (B) Study area map showing Soil Classes.

10991085, 2025, 9, Downloaded from https://onlinelibrary.wiley.com/doi/10.1002/hyp.70262 by INDIAN INSTITUTE OF TECHNOLOGY (NON -EAL), Wiley Online Library on [21/09/2025]. See the Terms and Conditions (https://onlinelibrary.wiley.com/terms-and-conditions) on Wiley Online Library for rules of use; OA articles are governed by the applicable Creative Commons License

and farming practices. This analysis is done using data sources of the Indian Meteorological Department (IMD), soil grid data, Land Use/Land Cover (LULC) data, and the Digital Elevation Model (DEM). In addition, the Sediment Delivery Ratio (SDR) was computed using the InVEST SDR model. Comprehensive details regarding the datasets employed in this study are given in Table 1.

2.3 | RUSLE Model Setup

This study examined soil erosion in the Jhelum Catchment using the Revised Universal Soil Loss Equation (RUSLE) model. The approach included comprehensive mapping of soil erosion across the Jhelum Basin, with calculations of the SDR and SSY carried out at the pixel level. The methodology, presented in Figure 2, highlights the application of Geographic Information System (GIS) tools for processing and visualising the data. The RUSLE model consists of five factors: rainfall erosivity (R), soil erodibility (K), slope length and steepness (LS), land cover (C), and support practices (P). These factors are combined to evaluate the potential annual soil loss (PSL), which is calculated using the formula: $\mathrm{PSL} = R \times K \times \mathrm{LS} \times C \times P$. This integrated method thoroughly assessed soil erosion by considering factors such as upslope areas, downslope flow paths, and the connectivity between erosion sources and

TABLE 1 | Details about the sources and spatial resolutions of the datasets used.

S. No	Data type	Specification	Range	Source
1	Soil Grids of ISRIC (International Soil Reference and Information Centre)	250 m	—	https://soilgrids.org/
2	General Circulation Models (GCM) (Coupled Model Intercomparison Project) (CMIP6)	Daily and monthly precipitation	2020–2090	World Climate Research Programme (WCRP) https://esgf-node.llnl.gov/search/cmip6/
3	Rainfall	0.25° × 0.25°	1960–2020, 1990–2022	IMD (Daily), Daily Gridded Rainfall Data and Indian Monsoon Data Assimilation and Analysis (IMDAA)
4	LULC	10 m	2017–2020	Sentinel-2 (ESRI)
5	Digital Elevation Model	10 m	2023	United States Geological Survey (USGS) Data

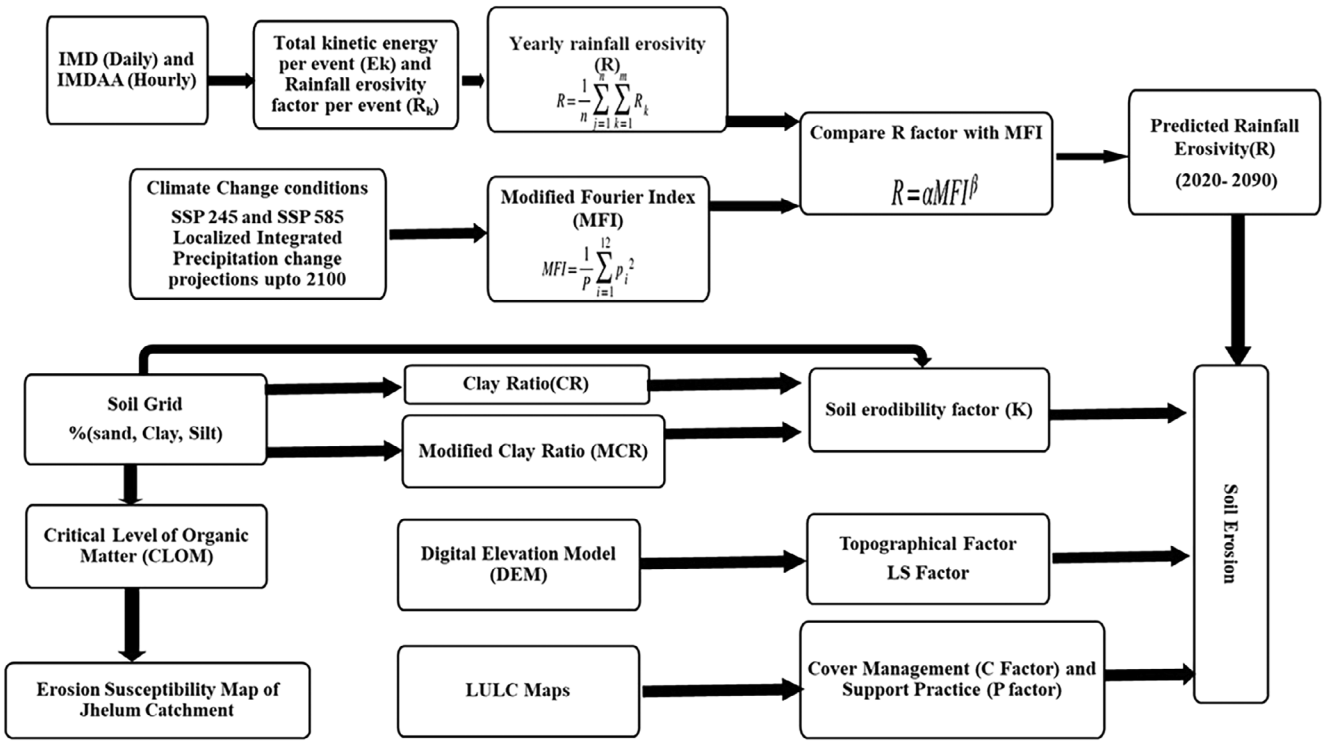

FIGURE 2 | Flowchart illustrating the methodology used in this study.

10991085, 2025, 9, Downloaded from https://onlinelibrary.wiley.com/doi/10.1002/hyp.70262 by INDIAN INSTITUTE OF TECHNOLOGY (NON -EAL), Wiley Online Library on [21/09/2025]. See the Terms and Conditions (https://onlinelibrary.wiley.com/terms-and-conditions) on Wiley Online Library for rules of use; OA articles are governed by the applicable Creative Commons License

deposition areas. IMD and CMIP6 climate data were analysed to assess and project rainfall from 2020 to 2090, examining the impact of climate change on soil erosion in the Jhelum catchment area. IMD and CMIP6 climate data were analysed to assess R and project R from 2020 to 2090, evaluating the impact of climate change on soil erosion patterns in the Jhelum catchment area.

2.3.1 | Rainfall Erosivity (*R*) Factor

This study employed two methods to calculate the *R* factors for the catchment area. The first method utilised high-resolution gridded precipitation data to determine the *R* factor, which is calculated as the product of a storm's total kinetic energy and the hourly rainfall intensity (Raj et al. 2022). For future projections of the *R* factor, an empirical equation was developed to estimate rainfall erosivity based on the Modified Fournier Index (MFI). This process included calculating both the Fournier Index (FI) and the MFI using daily precipitation datasets. The yearly averages of these indices were analysed to establish correlations with *R* factor values. This study addresses the limitations of General Circulation Models (GCMs) in assessing climate impacts on water resources at a regional scale by employing higher-resolution data and bias correction techniques. The delta change approach was used to incorporate GCM projections into catchment-scale analysis and hydrological modelling. This method applies correction factors derived from the correlation between GCMs and IMD data. The process involves computing bias factors in Python, adjusting historical data using change factors, and generating a transformed time series to represent future climate conditions (Islam and Chakma 2024b). Shared Socioeconomic Pathways (SSPs) represent different future socioeconomic and emission trajectories used in climate modelling. Two Shared Socioeconomic Pathways (SSP) scenarios, SSP245 and SSP585, representing moderate and high greenhouse gas emissions trajectories, are selected from the CMIP6 climate models. SSP245 represents a moderate emission scenario with greenhouse gas emissions peaking around 2040 and then declining, while SSP585 depicts a high-emission trajectory with continuous increases throughout the century. This study considers both scenarios to assess potential climate impacts on soil erosion, aiding decision-making and adaptation strategies for the Jhelum Catchment.

The MFI evaluates rainfall erosivity by analysing monthly precipitation in relation to the total annual precipitation. It is computed by adding the monthly precipitation values and dividing by the total annual precipitation. This method aligns with the approaches used in studies by Tiwari et al. (2016), Raj et al. (2022), and Islam and Chakma (2024b). The Equation (1) for the Modified Fournier Index is as follows:

$$\mathrm{MFI} = \frac{1}{P}\sum_{i=1}^{12} p_i^2 \tag{1}$$

P_i refers to the amount of precipitation in millimetres for a specific month (i), while P signifies the annual total precipitation in millimetres. The equation $R = \alpha \mathrm{MFI}^{\beta}$ defines the connection between R and the MFI. In this equation, α and β are coefficients, and r^2 represents the coefficient of determination, which measures how well the model fits the data. To calculate R, IMDAA data was used with MATLAB to determine the kinetic energy (ek) in MJ/ha/mm related to rainfall intensity (p) in mm/h, as shown in Equation (2) (Wischmeier and Smith 1958).

$$e_k = 0.119 + 0.0873\log(p), p \le 76\, e_k = 0.283, p > 76 \tag{2}$$

The rainfall erosivity factor (R_k) is calculated by multiplying the rainfall intensity (I_{60}) by the total kinetic energy (E_k) from each erosive event, expressed in megajoules per hectare (MJ/ha). The *R*-factor is represented in megajoules millimetres per hectare per hour (MJ-mm/ha/h). The annual rainfall erosivity (R), measured in MJ-mm/ha/h/year, is determined using Equation (3).

$$R = \frac{1}{n}\sum_{j=1}^{n}\sum_{k=1}^{m} R_k \tag{3}$$

In Equation (3), m refers to the number of erosive events in year j, while n indicates the total number of years in the dataset, 32 years in this study.

For Future prediction of rainfall erosivity, by calculating MFI and from the derived equation of R with MFI, rainfall erosivity of 2020 to 2090 every decade.

2.3.2 | Soil Erodibility (*K*) Factor

In the study, soil erodibility factors, known as *K*-factors, were determined using two methods: the Nomograph approach (KNOMO) and the EPIC model approach (KEPIC), as detailed by Ebabu et al. (2022). The Nomograph method considered various factors, including the proportions of sand, silt, and clay, as well as soil organic matter, permeability, and a soil structure classification. On the other hand, the EPIC model focused on the percentages of soil particle sizes along with soil organic carbon and other contributing aspects. Additionally, measures of erodibility such as the Clay Ratio (CR), Modified Clay Ratio (MCR), and Critical Level of Organic Matter (CLOM) were computed to determine the soil's vulnerability to erosion, using specific formulas and established threshold levels.

2.3.3 | *C* and *P* Factor

The Cover Management Factor (*C*-factor) and the Support Practice Factor (*P*-factor) are essential for assessing soil erosion susceptibility. The *C*-factor assesses how different cropping and management strategies influence erosion caused by water, relying on Land Use or Land Cover (LULC) data for evaluation (Renard et al. 1997). This study employed high-resolution Sentinel-2 LULC data, as illustrated in Figure 3, to assign *C*-factor values based on established recommendations in the literature (Chuenchum et al. 2020; Ganasri and Ramesh 2016; Pal and Chakrabortty 2019; Kaffas et al. 2021). *C*-factor values can vary from 0 to 0.45, based on the specific classifications of land use and land cover (LULC) (Kaffas et al. 2021). Conversely, the *P*-factor assesses how effective

10991085, 2025, 9, Downloaded from https://onlinelibrary.wiley.com/doi/10.1002/hyp.70262 by INDIAN INSTITUTE OF TECHNOLOGY (NON -EAL), Wiley Online Library on [21/09/2025]. See the Terms and Conditions (https://onlinelibrary.wiley.com/terms-and-conditions) on Wiley Online Library for rules of use; OA articles are governed by the applicable Creative Commons License

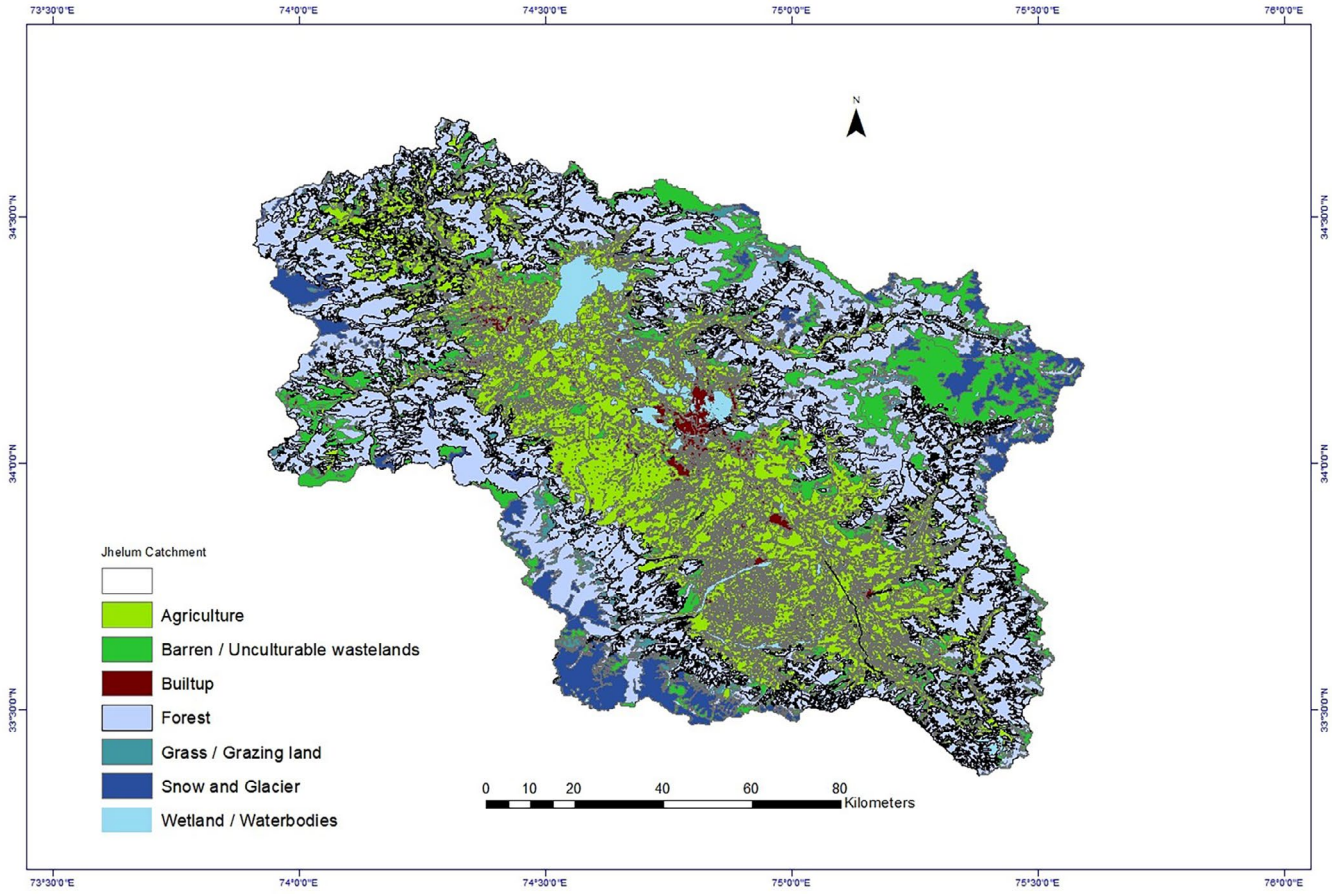

FIGURE 3 | Land Use Land Cover (LULC) map of the Jhelum Catchment for the year 2022.

agricultural support practices are in reducing soil loss, particularly concerning erosion from both upslope and downslope cultivation (Tsegaye and Bharti 2021). The *P*-factor plays a vital role in managing local soil erosion by influencing runoff and flow patterns (Tsegaye and Bharti 2021). In cases where specific management data are lacking, the *P*-factor is estimated using LULC data (Chuenchum et al. 2020; Ganasri and Ramesh 2016; Pal and Chakrabortty 2019). These factors offer a comprehensive view of soil erosion dynamics and help guide effective erosion control strategies. Figure 3 shows the LULC maps (2022) for the study area, while Table 2 lists the *C*-factor and *P*-factor values for various LULC categories. The classification accuracy for the Jhelum Catchment, assessed using Bhuvan LULC and Sentinel-2 data, reached 91.82% with an average Kappa Coefficient of 0.86, indicating significant accuracy within the 85% to 95% range (Anderson 1976).

TABLE 2 | *C*-factor and *P*-factor values for each LULC class.

S. No.	LULC type	LULC code	*C*-factor	*P* factor
1	Water	1	0	0
2	Trees	2	0.03	1
3	Flooded Vegetation	4	1	1
4	Crops	5	0.34	0.49
5	Built Area	7	0	0
6	Bare Ground	8	0.16	0.41
7	Snow/Ice	9	0	0
8	Rangeland	11	0.45	1

2.3.4 | LS Factor

In this study, the LS-factor, which evaluates the impact of terrain on soil erosion, was calculated using the LS-factor module of the QGIS Terrain Analysis—Hydrology tool. This module employs an algorithm inspired by the methods established by Desmet and Govers (1996), recognised for its effectiveness in modelling soil loss at the catchment scale. Panagos, Borrelli, and Meusburger (2015) and Panagos, Borrelli, Poesen, et al. (2015) utilised this algorithm to map the LS factor across European countries and other regions, highlighting its broader applicability beyond the original study.

2.3.5 | Sediment Delivery Ratio (SDR)

The Sediment Delivery Ratio (SDR) quantifies a watershed's efficiency in transporting soil particles from erosion-prone regions to

10991085, 2025, 9, Downloaded from https://onlinelibrary.wiley.com/doi/10.1002/hyp.70262 by INDIAN INSTITUTE OF TECHNOLOGY (NON -EAL), Wiley Online Library on [21/09/2025]. See the Terms and Conditions (https://onlinelibrary.wiley.com/terms-and-conditions) on Wiley Online Library for rules of use; OA articles are governed by the applicable Creative Commons License

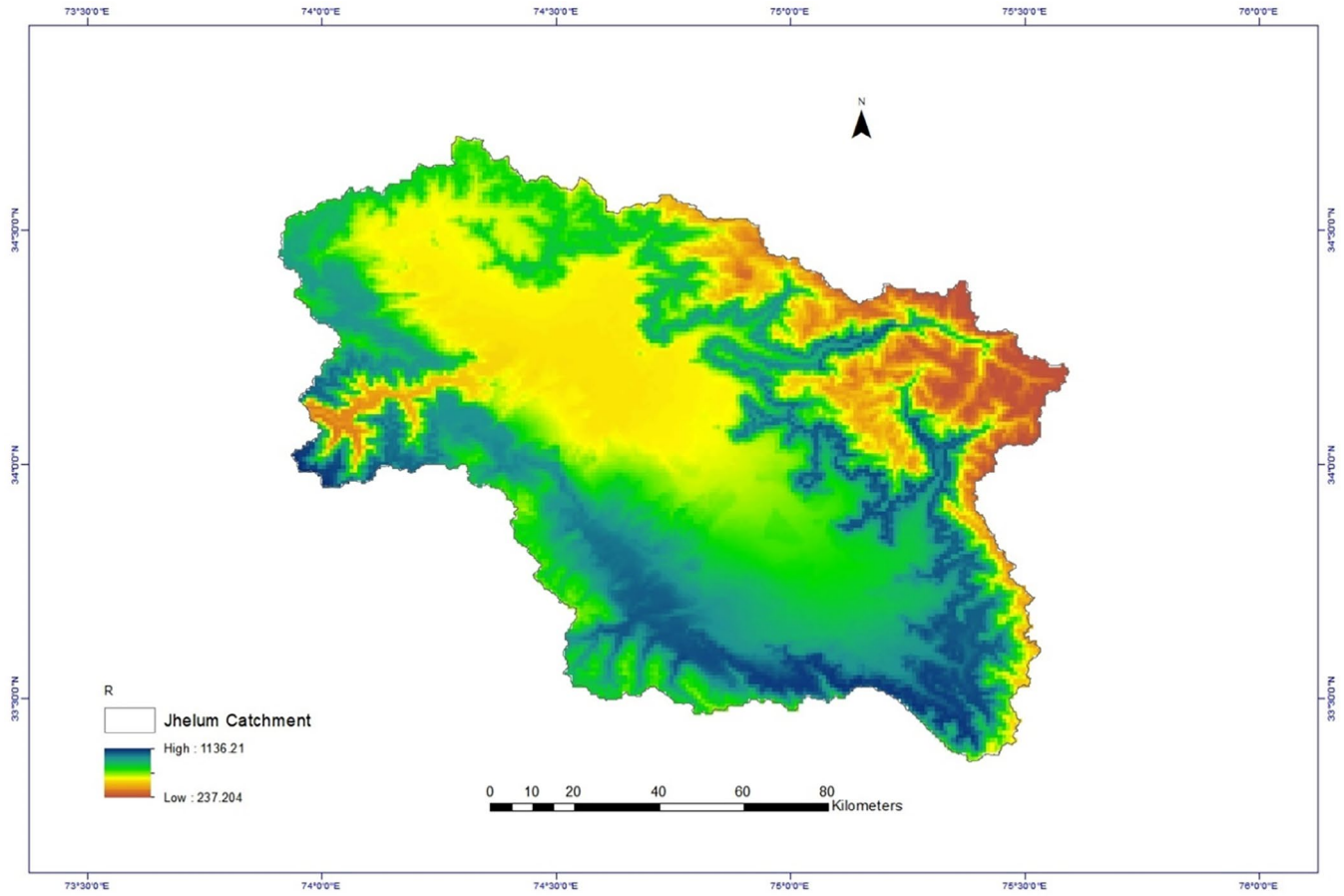

FIGURE 4 | Map of *R* (MJ-mm/ha/h/year) for the Jhelum Catchment (2020).

designated sites. This ratio is determined at the pixel level through the SDR module within the Integrated Valuation of Environmental Services and Trade-offs (InVEST) model. This model uses the Connection Index (CI) to estimate SDR values for each pixel, considering factors such as upslope area, downslope flow path, and terrain characteristics. This analysis provides insights into sediment connectivity, with higher values indicating a more significant potential for sediment transport. The SDR module aids in understanding sediment dynamics and contributes valuable information for soil conservation strategies within the watershed, offering a comprehensive view of sediment yield across the landscape (Kumar et al. 2022; Qin et al. 2018).

2.3.6 | Specific Sediment Yield (SSY)

RUSLE gives us the estimated soil erosion, represented by the Potential Soil Loss (PSL) values at each pixel. This soil loss then undergoes partial transport to downstream pixels. The net soil loss at each pixel or region is referred to as Specific Sediment Yield (SSY). The calculation of SSY involves multiplying PSL by the SDR, as expressed in Equation (4):

$$\text{SSY} = \text{PSL} \times \text{SDR} \tag{4}$$

SSY represents sediment yield or soil loss, measured in tons per hectare annually (t/ha/year).

2.3.7 | Trends in Soil Erosion From 2020 to 2090

This analysis examines trends in soil erosion from 2020 to 2090 across various land use categories, considering both SSP 245 and SSP 585 scenarios. The land use categories include Agriculture, Barren/Unculturable Wasteland, Built-up Areas, Forests, Grass/Grazing Land, Snow and Glaciers, and Wetlands/Water Bodies. The research reveals differences in soil erosion severity across various landscapes and climate scenarios, demonstrating how land use and changes in climate affect erosion dynamics over time.

Additionally, trends were analysed for various soil types, such as Cambisols, Lithosols, Glacial soils, and Inland Water, to understand how soil characteristics influence erosion patterns. This analysis provides key insights into future soil erosion patterns to support effective land management and conservation strategies.

3 | Results and Discussion

3.1 | *R* Factor

The *R* map for the Jhelum Catchment in 2020 is shown in Figure 4. The *R*-value was analysed with the MFI, and a scatter plot of *R* against MFI was created to determine the best-fit curve.

10991085, 2025, 9, Downloaded from https://onlinelibrary.wiley.com/doi/10.1002/hyp.70262 by INDIAN INSTITUTE OF TECHNOLOGY (NON-EAL), Wiley Online Library on [21/09/2025]. See the Terms and Conditions (https://onlinelibrary.wiley.com/terms-and-conditions) on Wiley Online Library for rules of use; OA articles are governed by the applicable Creative Commons License

The calculated constants α and β were 0.211822 and 1.7979, respectively, with a coefficient of determination (r^2) of 0.9425. The Equation (5) that describes the relationship between rainfall erosivity (R) and MFI for the Jhelum Catchment is as follows:

$$R = 0.211822\text{MFI}^{1.7979} \quad (5)$$

The MFI was computed for every decade from 2020 to 2090 using Python libraries and QGIS, based on the MPI-ESM1-2-LR model for both SSP245 and SSP585 scenarios. Furthermore, rainfall erosivity for each decade was estimated using an equation in the QGIS raster calculator.

The rainfall erosivity of MPI-ESM1-2-LR for every 10 years under both scenarios is depicted in Figure 5. MPI-ESM1-2-LR was selected because it correlated with IMD data in the Jhelum Catchment. The rationale behind choosing the MPI-ESM1-2-LR (SSP245 and SSP585 scenarios) is based on its moderate positive correlation coefficients with IMD precipitation data, which are 0.474379942 for SSP245 and 0.391730237 for SSP585. These coefficients indicate a reasonably good fit for capturing regional precipitation patterns, aiding in the analysis of soil erosion dynamics. The implications of these scenarios for soil erosion are significant as they provide projections of future climate conditions, which are crucial for predicting potential changes in soil erosion rates and patterns. The delta change technique was employed to address bias by incorporating variations between historical and projected climate data into the baseline conditions. This was done to ensure that the General Circulation Models (GCMs) projections were accurately integrated into the catchment-scale analysis and hydrological modelling. Specifically, the correction factors applied for MPI-ESM1-2-LR were 53.396 for SSP245 and 56.362 for SSP585. This method allowed for an effective integration of GCM outputs, providing reliable data for evaluating future soil erosion trends. The climate data was bias corrected as shown in Figure S1.

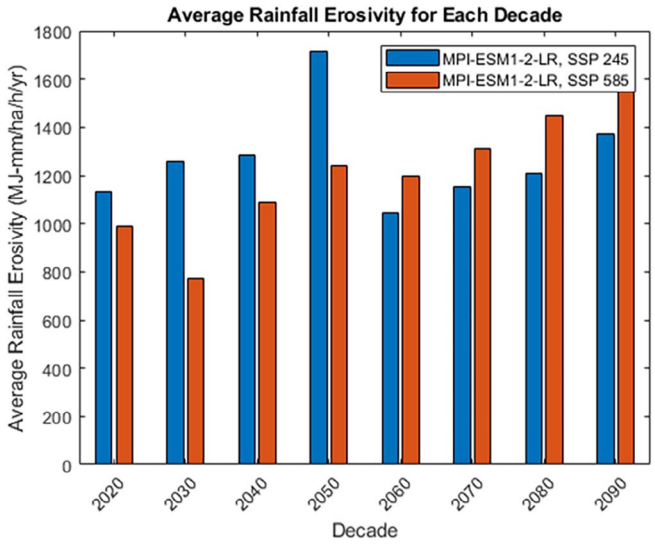

FIGURE 5 | The rainfall erosivity of MPI-ESM1-2-LR for every decade under both SSP scenarios.

3.2 | *K* Factor

To prepare the *K* factor map for the Jhelum Catchment, data for CR, MCR, and CLOM was prepared as shown in Figures S2, S3, and S4 (Supporting Information). The *K*-factor Map of the Jhelum Catchment is shown in Figure 6.

Evaluating the organic matter content in soil is essential for preventing erosion. Low levels of CLOM increase soil vulnerability to erosion. The CLOM ratio was analysed using soil particle data from India, as illustrated in Figure 8A. This index represents the level of organic matter, where higher CLOM values indicate a reduced risk of erosion. The CLOM map is classified to show how susceptible the soil is to erosion, following a method by (Pieri 2012). The CLOM index ranks soil susceptibility to erosion, indicating that CLOM values below 5% signify high susceptibility, values between 5% and 7% suggest moderate susceptibility, values from 7% to 9% denote low susceptibility and values exceeding 9% indicate stable conditions.

3.3 | *C*, *P* and LS Factors

The *C*-factor, *P*-factor, and LS-factor are shown in Figure 7A–C, respectively. These factors play a vital role in understanding soil erosion dynamics. The *C*-factor, which reflects Cover Management, has an average value of 0.173714 and can range from 0 to 0.45, representing various land cover conditions. This factor is important to understand the impact of land cover on soil erosion. The *P*-factor, representing Support Practices, has an average value of 0.623274, ranging from 0 to 1, indicating the efficiency of various practices in managing soil erosion and providing insights into soil conservation support practices. Lastly, the LS factor demonstrates a compelling average value of 11.4394, highlighting its significance and is a critical component representing Slope Length and Steepness, making a significant contribution to soil erosion assessments. The wide range of variability in the LS factor spans from 0.03009 to 1753.63062. This factor, representing Slope Length and Steepness, showcases diverse terrain characteristics across the studied area.

3.4 | Soil Erosion

The potential soil loss in the Jhelum catchment was analysed using RUSLE, as illustrated in Figure 7D. The variation in soil erosion rates highlights the necessity for targeted conservation efforts in key priority areas. A new classification system is introduced to assess the impact of soil erosion on agriculture and infrastructure. The classification, based on recommendations from previous studies, categorises erosion severity into six classes (E1 to E6) as applied by Aswathi et al. (2022); Guduru and Jilo (2023) with corresponding impacts on farming and infrastructure, providing a comprehensive evaluation tool for understanding the consequences of varying soil erosion levels. The annual soil loss severity classification (E1 to E6) indicates varying impacts. E1 (0–5 t/ha/year) signifies minimal erosion with limiting effects, while E2 (5–15 t/ha/year) poses a moderate risk to soil and agriculture. E3 (15–30 t/ha/year) represents significant erosion, causing immediate harm. E4 (30–50 t/ha/year) indicates severe erosion with significant agricultural reductions. E5 (50–100 t/ha/year) denotes severe

10991085, 2025, 9, Downloaded from https://onlinelibrary.wiley.com/doi/10.1002/hyp.70262 by INDIAN INSTITUTE OF TECHNOLOGY (NON-EAL), Wiley Online Library on [21/09/2025]. See the Terms and Conditions (https://onlinelibrary.wiley.com/terms-and-conditions) on Wiley Online Library for rules of use; OA articles are governed by the applicable Creative Commons License

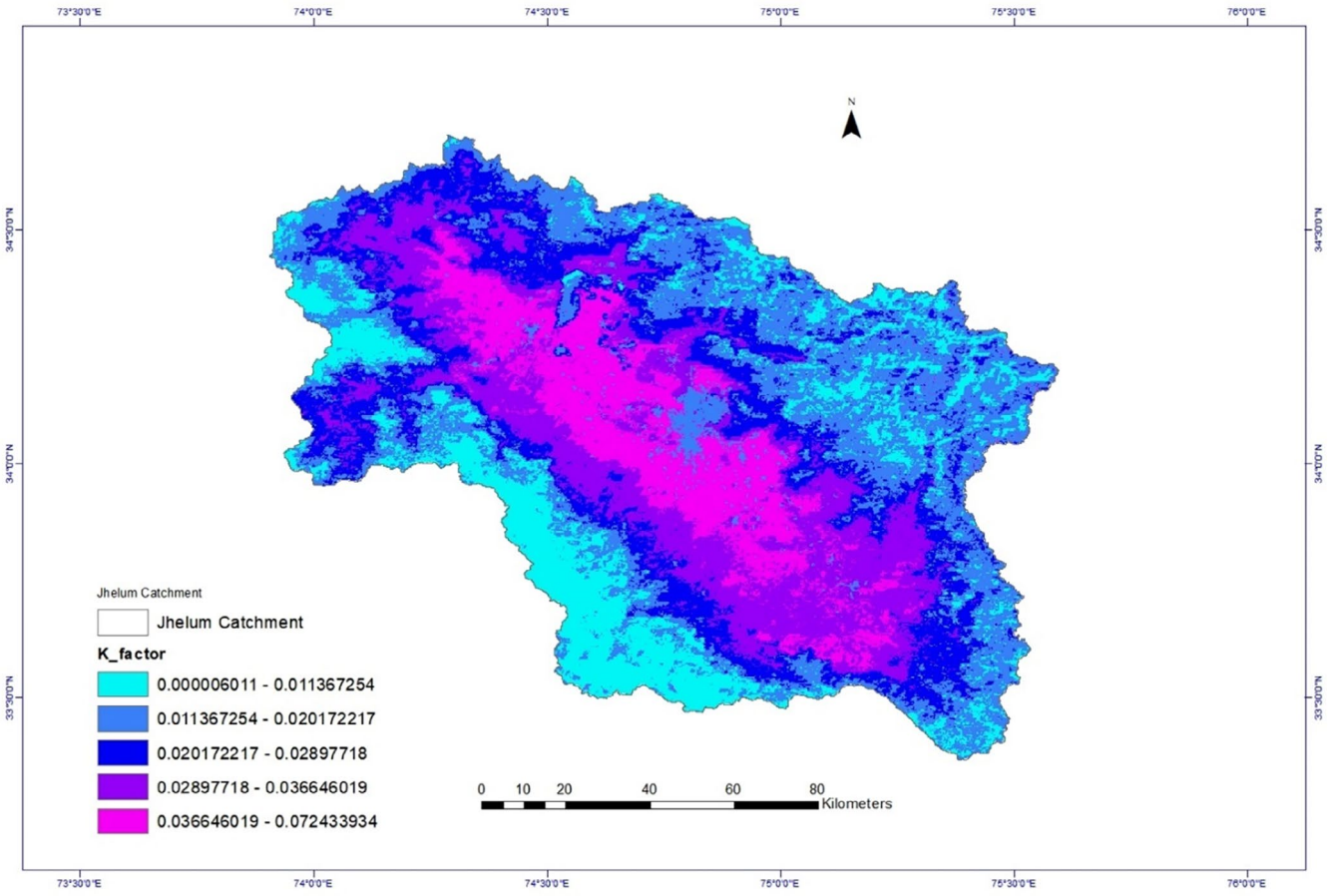

FIGURE 6 | The K factor Map (t-ha-h/ha/MJ/mm) of the Jhelum Catchment.

erosion, constraining land use. E6 (> 100 t/ha/year) signifies catastrophic erosion and extensive destruction. This classification aids in understanding the diverse impacts of soil erosion. From the RUSLE Equation, the Jhelum Catchment soil erosion map was prepared and classified into six severity classes, as shown in Figure 8B.

3.5 | Soil Erosion Projections

The percentage importance of each RUSLE factor was determined, and it was observed that for Jhelum Catchment, the most critical factor to predict soil erosion is *R* (Rainfall Erosivity), as shown in Figure S5. Further, Figures S6 and S7 show a rainfall erosivity map of each decade under SSP 245 and SSP 585. A soil erosion map for each decade under both scenarios was prepared. Figure S8 shows the soil erosion severity map for both scenarios for 2050 and 2090. Figures S9, S10, S11, S12, S13, S14, and S15 show the soil erosion severity map for 2020, highlighting severe erosion classes for 2020, 2030 (SSP245), 2030 (SSP585), 2050 (SSP245), 2050 (SSP585) 2090 (SSP245) and 2090 (SSP585) respectively. Projection of soil erosion class width was done based on LULC type and soil type from 2020 to 2090, and the results are shown in Figure 9. Figure 9A–H show trends in soil erosion from 2020 to 2090 for Agriculture, Barren/Unculturable Wasteland, Built-up Areas, Forest, Grass/Grazing Land, Snow and Glacier, and Wetland/Waterbodies respectively for both SSP 245 and SSP 585. Figure 9H–K show trends in soil erosion from 2020 to 2090 for Cambisols, Lithosols, Glaciers, and Inland Water, respectively, for both SSP 245 and SSP 585. Figure 9L predicted soil erosion of Jhelum Catchment up to 2090 under SSP245 and SSP 585 scenarios.

The study's quantitative analysis of soil erosion projections for the Jhelum Catchment (2020–2090) under SSP245 and SSP585 scenarios revealed a consistent upward trend in both maximum and mean soil erosion potential. SSP585 consistently demonstrated higher values than SSP245, emphasising the heightened impact under a high-emission trajectory. The increasing variability in soil erosion estimates, as indicated by rising standard deviation values, underscores the complexity and uncertainty associated with future projections. This emphasises the critical importance of implementing adaptive and proactive soil conservation measures to address the challenges of changing climate scenarios.

In this study, the sediment transport dynamics within the Jhelum Catchment were investigated by employing the InVEST SDR module. This module facilitated the generation of a comprehensive map illustrating the SDR across the catchment area. The SDR represents the proportion of soil particles eroded at a specific location that ultimately gets transported downstream. The resulting Sediment Delivery Map, depicted in Figure 8C, provides insights into the spatial distribution of sediment transport ratios, highlighting areas with varying degrees of erosion and deposition. Additionally, Figure 8D illustrates the Specific

10991085, 2025, 9, Downloaded from https://onlinelibrary.wiley.com/doi/10.1002/hyp.70262 by INDIAN INSTITUTE OF TECHNOLOGY (NON -EAL), Wiley Online Library on [21/09/2025]. See the Terms and Conditions (https://onlinelibrary.wiley.com/terms-and-conditions) on Wiley Online Library for rules of use; OA articles are governed by the applicable Creative Commons License

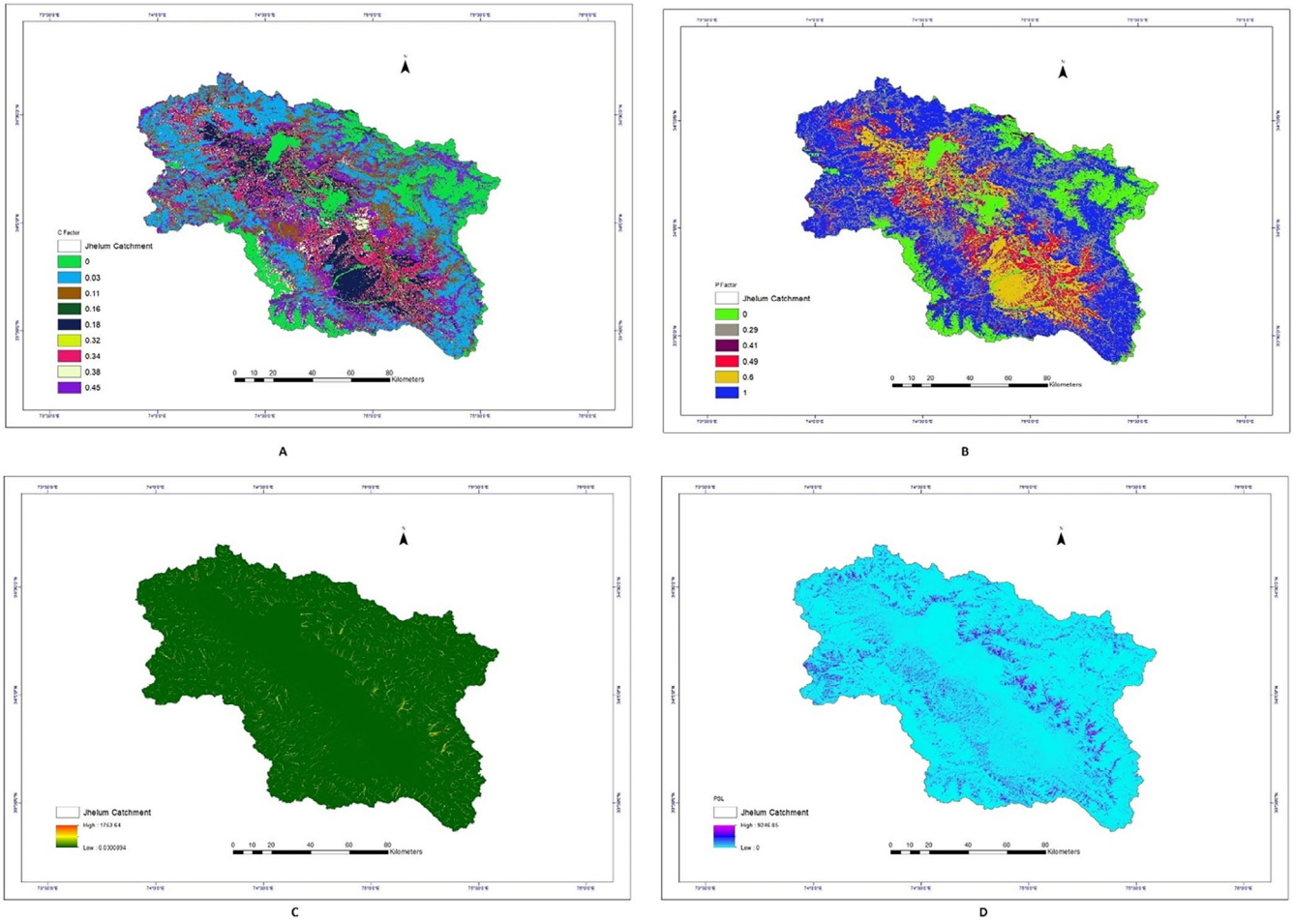

FIGURE 7 | (A) Map of the *C*-factor for the Jhelum catchment. (B) Map of the *P*-factor for the Jhelum catchment. (C) Map displaying the LS Factor for the Jhelum catchment. (D) Map illustrating PSL in the Jhelum catchment.

Sediment Yield (SSY), which quantifies the net soil loss or sediment yield at each pixel or region within the Jhelum Catchment. Together, these maps contribute to the understanding of sediment dynamics, which are crucial for watershed management and soil conservation.

3.6 | Discussion

The applicability of RUSLE in the Jhelum Catchment was enhanced through rigorous region-specific calibration using local soil, topography, climate, and land-use data. The model's accuracy and reliability were ensured by integrating high-resolution climate projections from CMIP6 and utilising advanced GIS-based analysis. This tailored approach highlights the robustness of RUSLE in predicting soil erosion under the unique conditions of the Jhelum Catchment.

This study measured the average rainfall erosivity at 777.79 MJ-mm/ha/h/year. This value was compared to the Indian rainfall erosivity data, which is reported to be 549.98 MJ-mm/ha/h/year. (Raj et al. 2022), and the global rainfall erosivity data, which stands at 1343.34 MJ-mm/ha/h/year. (Panagos et al. 2017). Additionally, the results were compared with the European Soil Data Centre's (ESDC) global projections for soil erosion by water in 2070 and the global rainfall erosivity forecasts for 2050 and 2070. The results in this study were 23% higher than the data provided by ESDC on request by the authors. This deviation in results is due to the resolution of global datasets. Furthermore, the value of $\alpha = 0.211822$ is notably lower compared to $\alpha = 0.38765$ reported by Islam and Chakma (2024b). This difference is attributable to data from only one general circulation model (GCM) used in this study. The mean values of the RUSLE parameters for the Jhelum Catchment provide critical insights into the soil erosion dynamics of the region. The high average LS factor (11.4394) indicates significant topographical variation, contributing to potential soil loss when combined with the rainfall erosivity (*R* factor = 777.7909 MJ-mm/ha/h/year) and soil erodibility ($K = 0.0228227$ t-ha-h/ha/MJ/mm). The values of average cover management (*C* factor = 0.173714) and support practice factor ($p = 0.623274$) suggest the current land cover and management practices are moderately effective in controlling erosion. However, the average sediment delivery ratio (SDR = 0.1565) and sediment yield (SSY = 6.6456 tons/ha/year) highlight sediment transport efficiency and the catchment's overall sediment yield. These findings indicate that the Jhelum catchment is increasingly vulnerable to intense rainfall-induced erosion events, situating it between national and global averages, and reflective of mountainous,

10991085, 2025, 9, Downloaded from https://onlinelibrary.wiley.com/doi/10.1002/hyp.70262 by INDIAN INSTITUTE OF TECHNOLOGY (NON -EAL), Wiley Online Library on [21/09/2025]. See the Terms and Conditions (https://onlinelibrary.wiley.com/terms-and-conditions) on Wiley Online Library for rules of use; OA articles are governed by the applicable Creative Commons License

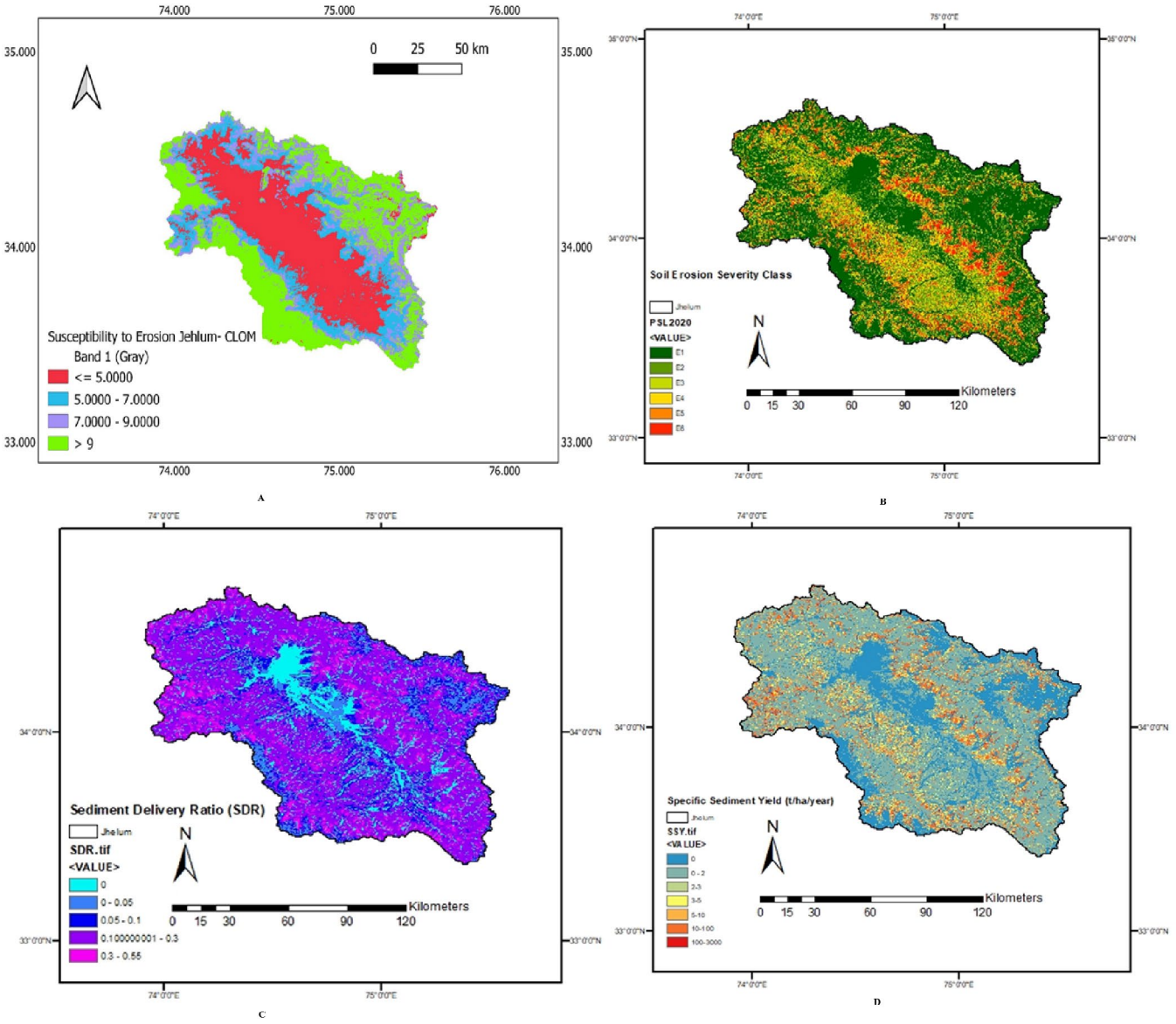

FIGURE 8 | (A) Susceptibility to Erosion -CLOM of Jhelum Catchment, (B) Soil Erosion severity map of Jhelum catchment, (C) Map showing the Sediment Delivery Ratio of the Jhelum Catchment and (D) Map showing Specific Sediment Yield (t/ha/year) of the Jhelum Catchment.

agriculturally transforming regions globally. Notably, Borrelli et al. (2020) projected a 60% global increase in soil erosion by 2070 under SSP5-RCP8.5 scenarios, which aligns with the upward trends identified in this study. These findings highlight the need for improved soil conservation strategies to manage and reduce soil erosion in the Jhelum Catchment effectively.

The study of soil erosion in the Jhelum Catchment from 2020 to 2090 shows a significant increase in soil loss under scenarios SSP245 and SSP585. The mean soil loss values exhibit a steady rise, with SSP585 projecting more severe erosion, peaking at 71.67 tons per hectare per year (t/ha/year) by 2090, compared to 51.54 t/ha/year under SSP245. Notably, 2050 marks a critical point under SSP245, with maximum and mean soil loss values reaching 10595.41 and 64.51 t/ha/year, respectively. The substantial variability in soil erosion rates, indicated by high standard deviation values, underscores the necessity for adaptive management strategies. Total annual soil loss projections are alarmingly high, with 126.30 million tons under SSP585 and 90.82 million tons under SSP245 by 2090, highlighting the escalating threat to agricultural productivity and land sustainability. Furthermore, the decreasing proportion of areas with less severe soil erosion over time suggests that regions previously less affected are becoming more prone to severe erosion, necessitating comprehensive soil management practices across the entire catchment. These findings underscore the urgent need for targeted soil conservation and climate-resilient land management to address soil erosion in the Jhelum Catchment.

Table 3 summarises the average values for the parameters of the RUSLE, as well as the SDR and SSY associated with the Jhelum Catchment. These average values provide crucial baseline information for future studies in a data-scarce region. They also guide sustainable land management practices and inform climate change impact assessments in the region.

Soil erosion rates escalated across all land use categories from 2020 to 2090, driven by intensified agricultural activities and

10991085, 2025, 9, Downloaded from https://onlinelibrary.wiley.com/doi/10.1002/hyp.70262 by INDIAN INSTITUTE OF TECHNOLOGY (NON -EAL), Wiley Online Library on [21/09/2025]. See the Terms and Conditions (https://onlinelibrary.wiley.com/terms-and-conditions) on Wiley Online Library for rules of use; OA articles are governed by the applicable Creative Commons License

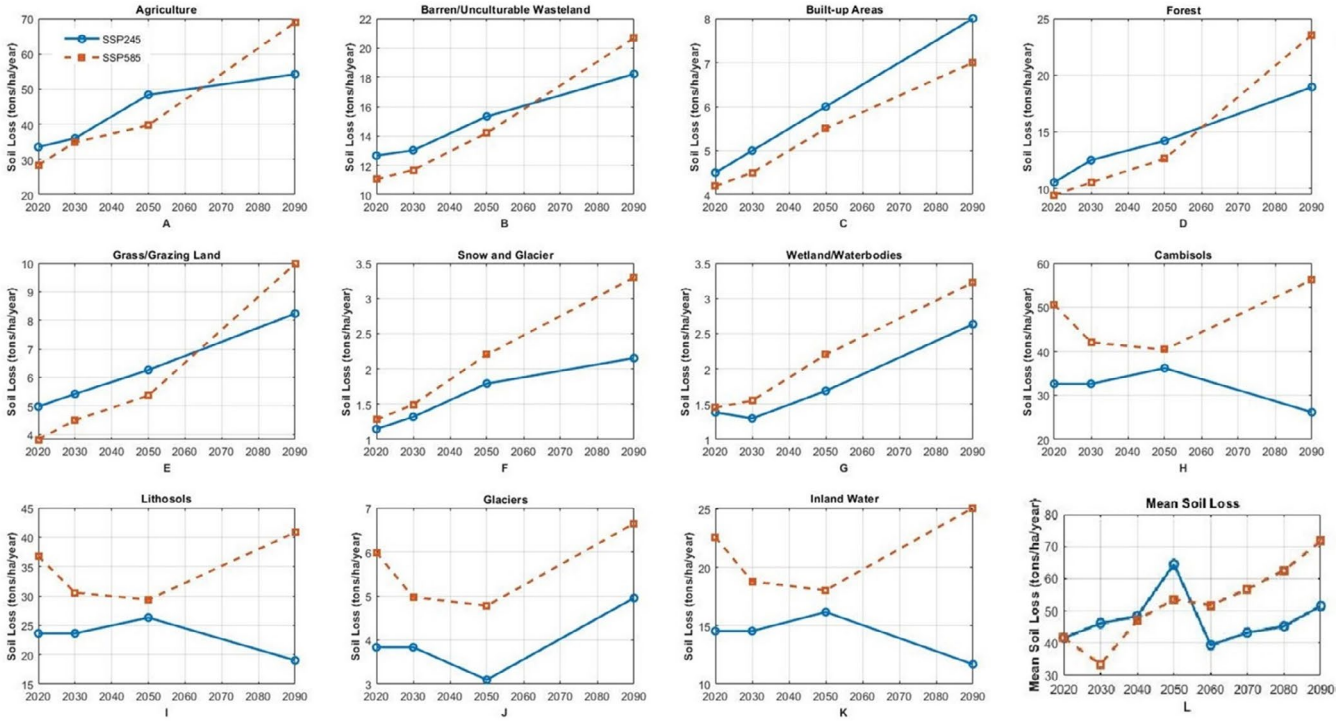

FIGURE 9 | Trends in soil erosion from 2020 to 2090 for Agriculture (A), Barren/Unculturable Wasteland (B), Built-up Areas (C), Forest (D), Grass/Grazing Land (E), Snow and Glacier (F), Wetland/Waterbodies (G). Cambisols (H), Lithosols (I), Glaciers (J), and Inland Water (K) respectively for both SSP 245 and SSP 585. (L) shows Predicted soil erosion of Jhelum Catchment up to 2090 under SSP245 and SSP 585 scenarios.

TABLE 3 | Average values of RUSLE parameters, SDR, and SSY for Jhelum Catchment.

S. No	Name	Average
1	*R* (MJ-mm/ha/h/year)	777.7909
2	*K* (t-ha-h/ha/MJ/mm)	0.0228227
3	*C*	0.173714
4	*P*	0.623274
5	LS	11.4394
6	PSL tons/ha/year	41.5976
7	SDR	0.156549
8	SSY (tons/ha/year)	6.6456

urban expansion. For instance, agricultural land saw a rise in erosion rates from 26.787 to 46.223 tons/ha/year under SSP245 and from 21.544 to 71.6736 tons/ha/year under SSP585. Cambisols consistently demonstrated higher soil loss than Lithosols and other soil types across scenarios, emphasising the critical influence of inherent soil characteristics on erosion susceptibility.

The results of this study reveal that both land use changes and climate variability will significantly amplify soil erosion across the Jhelum catchment, aligning with global findings that link anthropogenic pressures and climate change to increasing erosion risks (Borrelli et al. 2017; Chuenchum et al. 2020; Doulabian et al. 2021). The use of RUSLE integrated with high-resolution LULC and climate projections (SSPs) demonstrates methodological consistency with studies conducted in diverse global regions, such as the Heihe River Basin in China (Zhang et al. 2016) and the Nethravathi Basin in India (Ganasri and Ramesh 2016). The sharp increase in soil erosion under SSP5-8.5 is particularly concerning, as it reflects a broader global pattern of land degradation under high-emission scenarios (Pal and Chakrabortty 2019). These findings underscore the critical need for climate-resilient land use strategies and conservation practices. Additionally, the framework employed—combining RUSLE with GIS and remote sensing—has been widely used internationally (Maurya et al. 2021; Panagos, Borrelli, and Meusburger 2015; Panagos, Borrelli, Poesen, et al. 2015) reinforcing the global applicability of the approach. Wider implications include threats to agricultural productivity, water resources, and infrastructure, making this research relevant beyond the regional context. Although the projected rise in soil erosion in the Jhelum catchment may not be dramatic, it carries considerable uncertainty due to the reliance on long-term climate models and variable emission scenarios (Patro et al. 2022). Increased sediment flow into water bodies can lead to eutrophication (Ekholm and Lehtoranta 2012), obstruct river channels, elevate maintenance costs for infrastructure (Panagos et al. 2024), and increase flood risks (Olorunfemi et al. 2020). Similar soil erosion concerns have been observed across diverse global contexts, reinforcing the broader applicability of this study's findings. Hydrological connectivity offers insight into how spatial linkages influence runoff and sediment transport (Bracken and Croke 2007). For instance, in the Ethiopian Highlands, Hurni et al. (2005) documented accelerated erosion linked to agricultural expansion and rainfall variability, while Le Roux (2011) highlighted the

10991085, 2025, 9, Downloaded from https://onlinelibrary.wiley.com/doi/10.1002/hyp.70262 by INDIAN INSTITUTE OF TECHNOLOGY (NON-EAL), Wiley Online Library on [21/09/2025]. See the Terms and Conditions (https://onlinelibrary.wiley.com/terms-and-conditions) on Wiley Online Library for rules of use; OA articles are governed by the applicable Creative Commons License

role of land cover degradation in increasing sediment yields in South Africa. In the Andes of Colombia, Hoyos (2005) used spatial modelling to reveal how topography and land use patterns interact to influence erosion intensity. Similar methodologies have been applied in sub-Saharan Africa (Karamage et al. 2017), emphasising the global utility of integrating RUSLE with GIS and remote sensing in erosion modelling. In large transboundary basins like the Nile (Haregeweyn et al. 2017) and the Mekong (Shrestha et al. 2013), land use-driven erosion and sediment transport have raised transnational water governance challenges. Panagos et al. (2022) emphasised the need for pan-European harmonisation of soil conservation under climate pressures, further validating the present study's approach. Likewise, studies in temperate regions such as Scotland (Tetzlaff et al. 2009) and Bracken and Croke (2007) have revealed how hillslope-channel connectivity intensifies sediment yields—a mechanism directly comparable to those observed in the Upper Jhelum region. Similar findings have emerged from the Mediterranean (Munoz 2025), where rainfall erosivity trends were offset by localised management efforts, and across the EU, where effective soil governance has mitigated degradation risks (Efthimiou 2025). Shojaeezadeh et al. (2024) highlighted increased soil erosion risks in the U.S. due to climate change, underscoring the relevance of proactive conservation measures. Furthermore, modelling studies in the Abaya-Chamo Sub-Basin in Ethiopia (Alemu et al. 2025) and susceptibility mapping in North Africa (Salhi et al. 2025) reinforce the global relevance of integrating RUSLE with GIS and remote sensing for erosion prediction and landscape management. These parallels demonstrate that the modelling framework employed here can inform soil and water conservation planning worldwide, particularly in data-scarce mountainous or tropical regions. Moreover, erosion-induced sedimentation in critical water infrastructure has been reported in Turkey (Altinbilek 2002), Switzerland (Delaney et al. 2024), Italy (Patro et al. 2022), the USA (Graf et al. 2010), and Africa (Fenta et al. 2020), underscoring the urgent need for globally coordinated erosion control strategies. These findings underscore the broader relevance of understanding rainfall–soil–land cover interactions for erosion prediction and control, especially under intensifying climate extremes. The findings of this study help identify erosion-prone zones, enabling evidence-based planning and decision-making (Panagos, Borrelli, and Meusburger 2015, Panagos, Borrelli, Poesen, et al. 2015; Ganasri and Ramesh 2016). They hold particular relevance for India's Dam Rehabilitation and Improvement Project (DRIP) (Pillai and Giraud 2014), contribute to global soil conservation strategies (Borrelli et al. 2017), and advance the United Nations Sustainable Development Goals—especially SDG 2 (Zero Hunger), SDG 6 (Clean Water and Sanitation), SDG 13 (Climate Action), and SDG 15 (Life on Land) (United Nations 2015). Efficient monitoring systems are crucial for supporting mitigation strategies such as the construction of check dams and the efficient removal of sediment. Integrating remote sensing technologies—including optical imagery, synthetic aperture radar (SAR), and satellite altimetry—can significantly enhance the analysis of spatial and temporal sedimentation patterns. Overall, this research provides scalable insights for climate-resilient, sustainable land and water resource management at both regional and global levels. The modelling approach used here can be adopted in other data-scarce basins, contributing to global efforts in sustainable watershed management and soil conservation planning.

3.7 | Future Scope and Limitations

A limitation of this study is the use of a single General Circulation Model (GCM), selected for its best correlation with IMD data. While this GCM provides valuable insights, it may not fully represent the range of regional climate variability. Additionally, the study relies on national and global gridded datasets due to the absence of extensive local ground measurements, which can introduce interpolation errors. Future research could improve accuracy by integrating data from multiple GCMs and incorporating more localised observations to capture soil erosion dynamics better. Future research should investigate how land use, soil properties, and vegetation affect soil erosion trends. The reliance on national and global gridded datasets may introduce interpolation errors, potentially affecting model accuracy. Additionally, soil erosion trends are influenced by soil properties and vegetation cover, but limited high-resolution data constrains a more precise assessment. This study serves as a foundation for analysing the impact of climate change on RUSLE parameters and suggests exploring land management practices, extreme weather events, and erosion control strategies.

4 | Conclusions

In conclusion, this research indicates a significant increase in soil erosion in the Jhelum Catchment from 2020 to 2090, with the SSP585 scenario showing greater severity than the SSP245 scenario. This underscores the urgent need for proactive interventions and sustainable land management practices.

The assessment of erosion severity, ranging from Minor to Catastrophic, highlights that areas classified as less severe in 2020 are expected to worsen significantly in the future. This study serves as the first comprehensive investigation of the region, providing a foundation for future research.

1. SSP585 projections consistently show a more severe trend, suggesting intensified soil erosion impacts on the catchment.
2. The classification into erosion severity classes (Minor to Catastrophic) provides a qualitative assessment of potential impacts.
3. Zones categorised as less severe in 2020 demonstrate a significant worsening trend in the future, reflecting the dynamic nature of soil erosion.
4. Mapping RUSLE factors, SDR, and SSY, along with soil erosion projections up to 2090 for the SSP245 and SSP585 scenarios, provides a valuable methodology for similar regions.
5. Average values of all RUSLE Factors are given for future research in this data-scarce region.
6. The Jhelum Catchment's high R and LS factors and moderate C and P result in substantial sediment yield (6.6456 tons/ha/year) and sediment delivery ratio (0.1565).

10991085, 2025, 9, Downloaded from https://onlinelibrary.wiley.com/doi/10.1002/hyp.70262 by INDIAN INSTITUTE OF TECHNOLOGY (NON-EAL), Wiley Online Library on [21/09/2025]. See the Terms and Conditions (https://onlinelibrary.wiley.com/terms-and-conditions) on Wiley Online Library for rules of use; OA articles are governed by the applicable Creative Commons License

The results reveal a significant risk of erosion and sediment transport in the steep terrain of the Jhelum Catchment, highlighting the urgent need for effective land management. To combat increasing soil erosion in the area, the study advocates for immediate policies and measures. Key recommendations include implementing soil conservation practices such as terracing and reforestation, enhancing land management strategies, and adopting climate-resilient agricultural practices. Additionally, strengthening monitoring systems for soil erosion and utilising real-time data for adaptive management are crucial. This study enhances our understanding of soil erosion dynamics by mapping factors like the Revised Universal Soil Loss Equation (RUSLE), Sediment Delivery Ratio (SDR), and Soil Suspended Yield (SSY). This study enhances our understanding of hydrological processes by comprehensively integrating rainfall erosivity and sediment delivery through RUSLE and the InVEST SDR model. The *R*-factor quantifies rainfall's erosive potential via storm intensity, duration, and kinetic energy, driving soil detachment, while the SDR component spatially represents how hydrological connectivity and topographic controls govern sediment transport. By linking soil erosion with sediment export pathways, the study offers a process-based, spatially explicit framework for assessing sediment dynamics under varying land use and hydrological conditions. This study shows that future increased rainfall will intensify soil erosion and sediment yield in the Jhelum Catchment, affecting runoff and sediment transport dynamics. The RUSLE-based framework provides critical insights for similar basins, emphasising the need for adaptive erosion control strategies to mitigate hydrological impacts in a changing climate. The findings underscore the importance of strategic conservation measures in the face of changing climate conditions and offer valuable insights for future research on land management practices and erosion control strategies.

Acknowledgements

The authors would like to thank the India Meteorology Department (IMD), the International Soil Reference and Information Centre, and the CMIP6 models obtained from the CMIP6 data portal (https://esgf-node.llnl.gov/projects/cmip6/), as well as the NASA Centre for Climate Simulation (NCCS) for providing crucial data. Special thanks are extended to the European Soil Data Centre (ESDC) for contributing datasets related to global soil erosion by water for the year 2070, as well as projections of global rainfall erosivity for the years 2050 and 2070. Epari Ritesh Patro acknowledges the funding support from the Maa- ja vesitekniikan tuki ry's RUPIAH project (#44943).

Conflicts of Interest

The authors declare no conflicts of interest.

Data Availability Statement

The data that support the findings of this study are available from the corresponding author upon reasonable request.

References

Aghsaei, H., N. Mobarghaee Dinan, A. Moridi, et al. 2020. "Effects of Dynamic Land Use/Land Cover Change on Water Resources and Sediment Yield in the Anzali Wetland Catchment, Gilan, Iran." *Science of the Total Environment* 712: 136449. https://doi.org/10.1016/j.scitotenv.2019.136449.

Alemu, M. D., F. Laekemariam, S. Belay, J. Van Tol, and A. G. Mengistu. 2025. "Modeling Soil Erosion for Sustainable Landscape Management Using RUSLE in the Landscapes of Abaya-Chamo Sub-Basin, Ethiopia." *Modeling Earth Systems and Environment* 11, no. 3: 171.

Altinbilek, D. 2002. "The Role of Dams in Development." *Water Science and Technology* 45, no. 8: 169–180.

Anderson, J. A. 1976. *Land Use and Land Cover Classification System for Use With Remote Sensor Data*. USGS.

Asheghi, R., and S. A. Hosseini. 2020. "Prediction of Bed Load Sediments Using Different Artificial Neural Network Models." *Frontiers of Structural and Civil Engineering* 14, no. 2: 374–386. https://doi.org/10.1007/s11709-019-0600-0.

Aswathi, J., K. S. Sajinkumar, A. Rajaneesh, et al. 2022. "Furthering the Precision of RUSLE Soil Erosion With PSInSAR Data: An Innovative Model." *Geocarto International* 37, no. 27: 16108–16131. https://doi.org/10.1080/10106049.2022.2105407.

Avand, M., M. Mohammadi, F. Mirchooli, A. Kavian, and J. P. Tiefenbacher. 2023. "A New Approach for Smart Soil Erosion Modeling: Integration of Empirical and Machine-Learning Models." *Environmental Modeling & Assessment* 28, no. 1: 145–160.

Berger, M., J. Campos, M. Carolli, et al. 2021. "Advancing the Water Footprint Into an Instrument to Support Achieving the SDGs – Recommendations From the "Water as a Global Resources" Research Initiative (GRoW)." *Water Resources Management* 35, no. 4: 1291–1298. https://doi.org/10.1007/s11269-021-02784-9.

Bhat, M. S., A. Alam, B. Ahmad, et al. 2019. "Flood Frequency Analysis of River Jhelum in Kashmir Basin." *Quaternary International* 507: 288–294. https://doi.org/10.1016/j.quaint.2018.09.039.

Bhat, M. S., A. Alam, S. Ahmad, H. Farooq, and B. Ahmad. 2019. "Flood Hazard Assessment of Upper Jhelum Basin Using Morphometric Parameters." *Environmental Earth Sciences* 78, no. 2: 54. https://doi.org/10.1007/s12665-019-8046-1.

Bhatt, C. M., G. S. Rao, M. Farooq, et al. 2017. "Satellite-Based Assessment of the Catastrophic Jhelum Floods of September 2014, Jammu & Kashmir, India." *Geomatics, Natural Hazards and Risk* 8, no. 2: 309–327. https://doi.org/10.1080/19475705.2016.1218943.

Bhutiyani, M. R., V. S. Kale, and N. J. Pawar. 2007. "Long-Term Trends in Maximum, Minimum, and Mean Annual Air Temperatures Across the Northwestern Himalayas During the Twentieth Century." *Climatic Change* 85, no. 1: 159–177.

Borrelli, P., D. A. Robinson, L. R. Fleischer, et al. 2017. "An Assessment of the Global Impact of 21st Century Land Use Change on Soil Erosion." *Nature Communications* 8, no. 1: 2013. https://doi.org/10.1038/s41467-017-02142-7.

Borrelli, P., D. A. Robinson, P. Panagos, et al. 2020. "Land Use and Climate Change Impacts on Global Soil Erosion by Water (2015–2070)." *Proceedings of the National Academy of Sciences* 117, no. 36: 21994–22001. https://doi.org/10.1073/pnas.2001403117.

Bracken, L. J., and J. Croke. 2007. "The Concept of Hydrological Connectivity and Its Contribution to Understanding Runoff-Dominated Geomorphic Systems." *Hydrological Processes* 21, no. 13: 1749–1763.

Chuenchum, P., M. Xu, and W. Tang. 2020. "Predicted Trends of Soil Erosion and Sediment Yield From Future Land Use and Climate Change Scenarios in the Lancang–Mekong River by Using the Modified RUSLE Model." *International Soil and Water Conservation Research* 8, no. 3: 213–227. https://doi.org/10.1016/j.iswcr.2020.06.006.

DeFries, R., and K. N. Eshleman. 2004. "Land-Use Change and Hydrologic Processes: A Major Focus for the Future." *Hydrological Processes* 18, no. 11: 2183–2186. https://doi.org/10.1002/hyp.5584.

Delaney, I., M. A. Werder, D. Felix, I. Albayrak, R. M. Boes, and D. Farinotti. 2024. "Controls on Sediment Transport From a Glacierized Catchment in the Swiss Alps Established Through Inverse Modeling

10991085, 2025, 9, Downloaded from https://onlinelibrary.wiley.com/doi/10.1002/hyp.70262 by INDIAN INSTITUTE OF TECHNOLOGY (NON-EAL), Wiley Online Library on [21/09/2025]. See the Terms and Conditions (https://onlinelibrary.wiley.com/terms-and-conditions) on Wiley Online Library for rules of use; OA articles are governed by the applicable Creative Commons License

of Geomorphic Processes." *Water Resources Research* 60, no. 4: e2023WR035589.

Desmet, P. J. J., and G. Govers. 1996. "A GIS Procedure for Automatically Calculating the USLE LS Factor on Topographically Complex Landscape Units." *Journal of Soil and Water Conservation* 51, no. 5: 427–433. http://www.jswconline.org/content/51/5/427.abstract.

Dhakal, S. 2015. *Evolution of Geomorphologic Hazards in Hindu Kush Himalaya*, 53–72. Springer. https://doi.org/10.1007/978-4-431-55242-0_4.

Doulabian, S., A. Shadmehri Toosi, G. Humberto Calbimonte, E. Ghasemi Tousi, and S. Alaghmand. 2021. "Projected Climate Change Impacts on Soil Erosion Over Iran." *Journal of Hydrology* 598: 126432. https://doi.org/10.1016/j.jhydrol.2021.126432.

Dutta, S. 2016. "Soil Erosion, Sediment Yield and Sedimentation of Reservoir: A Review." *Modeling Earth Systems and Environment* 2, no. 3: 123. https://doi.org/10.1007/s40808-016-0182-y.

Ebabu, K., A. Tsunekawa, N. Haregeweyn, et al. 2022. "Global Analysis of Cover Management and Support Practice Factors That Control Soil Erosion and Conservation." *International Soil and Water Conservation Research* 10, no. 2: 161–176. https://doi.org/10.1016/j.iswcr.2021.12.002.

Efthimiou, N. 2025. "Governance and Degradation of Soil in the EU. An Overview of Policies With a Focus on Soil Erosion." *Soil and Tillage Research* 245: 106308.

Ekholm, P., and J. Lehtoranta. 2012. "Does Control of Soil Erosion Inhibit Aquatic Eutrophication?" *Journal of Environmental Management* 93, no. 1: 140–146.

Fenta, A. A., A. Tsunekawa, N. Haregeweyn, et al. 2020. "Land Susceptibility to Water and Wind Erosion Risks in the East Africa Region." *Science of the Total Environment* 703: 135016.

Ganaie, T. A., M. Sahana, and H. Hashia. 2018. "Assessing and Monitoring the Human Influence on Water Quality in Response to Land Transformation Within the Wular Environs of Kashmir Valley." *GeoJournal* 83, no. 5: 1091–1113. https://doi.org/10.1007/s10708-017-9822-7.

Ganasri, B. P., and H. Ramesh. 2016. "Assessment of Soil Erosion by RUSLE Model Using Remote Sensing and GIS - A Case Study of Nethravathi Basin." *Geoscience Frontiers* 7, no. 6: 953–961. https://doi.org/10.1016/j.gsf.2015.10.007.

Genxu, W., Y. Lingyuan, C. Lin, and J. Kubota. 2005. "Impacts of Land Use Changes on Groundwater Resources in the Heihe River Basin." *Journal of Geographical Sciences* 15, no. 4: 405–414. https://doi.org/10.1007/BF02892147.

Gholami, V., H. Sahour, and M. A. Hadian. 2020. "Mapping Soil Erosion Rates Using Self-Organizing Map (SOM) and Geographic Information System (GIS) on Hillslopes." *Earth Science Informatics* 13: 1175–1185. https://doi.org/10.1007/s12145-020-00499-w.

Graf, W. L., E. Wohl, T. Sinha, and J. L. Sabo. 2010. "Sedimentation and Sustainability of Western American Reservoirs." *Water Resources Research* 46, no. 12: 1–13. https://doi.org/10.1029/2009WR008836.

Guduru, J. U., and N. B. Jilo. 2023. "Assessment of Rainfall-Induced Soil Erosion Rate and Severity Analysis for Prioritization of Conservation Measures Using RUSLE and Multi-Criteria Evaluations Technique at Gidabo Watershed, Rift Valley Basin, Ethiopia." *Ecohydrology & Hydrobiology* 23, no. 1: 30–47. https://doi.org/10.1016/j.ecohyd.2022.09.002.

Haregeweyn, N., A. Tsunekawa, J. Poesen, et al. 2017. "Comprehensive Assessment of Soil Erosion Risk for Better Land Use Planning in River Basins: Case Study of the Upper Blue Nile River." *Science of the Total Environment* 574: 95–108.

Hou, S., Y. Yu, and Q. Wang. 2024. "Predictive Modeling of Diverse Factors Impacting Regional Soil Erosion Degree With Machine Learning." *Earth Science Informatics* 17: 3039–3051. https://doi.org/10.1007/s12145-024-01329-z.

Hoyos, N. 2005. "Spatial Modeling of Soil Erosion Potential in a Tropical Watershed of the Colombian Andes." *Catena* 63, no. 1: 85–108.

Hurni, H., K. Tato, and G. Zeleke. 2005. "The Implications of Changes in Population, Land Use, and Land Management for Surface Runoff in the Upper Nile Basin Area of Ethiopia." *Mountain Research and Development* 25, no. 2: 147–154.

Islam, S. U., and S. Chakma. 2024a. "Impact of LULC Changes on Hydrological Flow Regimes and Runoff Coefficient in Upper Jhelum Basin, India." *Sustainable Water Resources Management* 10, no. 1: 1–15. https://doi.org/10.1007/s40899-023-00987-z2024a.

Islam, S. U., and S. Chakma. 2024b. "Evaluating the Long-Term Influence of Climate Change on Rainfall Erosivity in the Jhelum Catchment: A GCM-Based Analysis." *Environment, Development and Sustainability* 27: 1–18. https://doi.org/10.1007/s10668-024-05286-x.

Kaffas, K., V. Pisinaras, M. J. Al Sayah, S. Santopietro, and M. Righetti. 2021. "A USLE-Based Model With Modified LS-Factor and Sediment Delivery Module for Alpine Basins." *Catena* 207: 105655. https://doi.org/10.1016/j.catena.2021.105655.

Kalantari, Z., S. W. Lyon, L. Folkeson, et al. 2014. "Quantifying the Hydrological Impact of Simulated Changes in Land Use on Peak Discharge in a Small Catchment." *Science of the Total Environment* 466–467: 741–754. https://doi.org/10.1016/j.scitotenv.2013.07.047.

Karamage, F., C. Zhang, T. Liu, A. Maganda, and A. Isabwe. 2017. "Soil Erosion Risk Assessment in Uganda." *Forests* 8, no. 2: 52.

Khanday, S. A., S. U. Bhat, S. T. Islam, and I. Sabha. 2021. "Identifying Lithogenic and Anthropogenic Factors Responsible for Spatio-Seasonal Patterns and Quality Evaluation of Snow Melt Waters of the River Jhelum Basin in Kashmir Himalaya." *Catena* 196: 104853. https://doi.org/10.1016/j.catena.2020.104853.

Kothyari, U. C. 2009. *Sediment Problems and Management in Asian River Basins*. Vol. 349. IAHS Publishes.

Kothyari, U. C., M. K. Jain, and K. G. Ranga Raju. 2002. "Estimation de la Variation Temporelle de L'exportation Sédimentaire Grâce à un SIG." *Hydrological Sciences Journal* 47, no. 5: 693–706. https://doi.org/10.1080/02626660209492974.

Kumar, M., A. P. Sahu, N. Sahoo, S. S. Dash, S. K. Raul, and B. Panigrahi. 2022. "Global-Scale Application of the RUSLE Model: A Comprehensive Review." *Hydrological Sciences Journal* 67, no. 5: 806–830. https://doi.org/10.1080/02626667.2021.2020277.

Lampert, A. 2019. "Over-Exploitation of Natural Resources Is Followed by Inevitable Declines in Economic Growth and Discount Rate." *Nature Communications* 10, no. 1: 1419. https://doi.org/10.1038/s41467-019-09246-2.

Le Roux, J. J. 2011. "Monitoring Soil Erosion in South Africa at a Regional Scale." *Geohazards Project Report for the Council of Geoscience; ARC-ISCW Report No. GW/A/2011/23 Project GW*, *59*(004).

Li, L., Y. Wang, and C. Liu. 2014. "Effects of Land Use Changes on Soil Erosion in a Fast Developing Area." *International Journal of Environmental Science and Technology* 11: 1549–1562. https://doi.org/10.1007/s13762-013-0341-x.

Maurya, S., P. K. Srivastava, A. Yaduvanshi, et al. 2021. "Soil Erosion in Future Scenario Using CMIP5 Models and Earth Observation Datasets." *Journal of Hydrology* 594: 125851. https://doi.org/10.1016/j.jhydrol.2020.125851.

Meraj, G., S. A. Romshoo, S. Ayoub, and S. Altaf. 2018. "Geoinformatics Based Approach for Estimating the Sediment Yield of the Mountainous Watersheds in Kashmir Himalaya, India." *Geocarto International* 33, no. 10: 1114–1138. https://doi.org/10.1080/10106049.2017.1333536.

Munoz, M. Á. B. 2025. "Positive Rainfall Erosivity Trends Compared With the Reduction in Soil Erosion in a Mediterranean Area (1996–2020)." *Catena* 249: 108606.

10991085, 2025, 9, Downloaded from https://onlinelibrary.wiley.com/doi/10.1002/hyp.70262 by INDIAN INSTITUTE OF TECHNOLOGY (NON-EAL), Wiley Online Library on [21/09/2025]. See the Terms and Conditions (https://onlinelibrary.wiley.com/terms-and-conditions) on Wiley Online Library for rules of use; OA articles are governed by the applicable Creative Commons License

Olorunfemi, I. E., A. A. Komolafe, J. T. Fasinmirin, A. A. Olufayo, and S. O. Akande. 2020. "A GIS-Based Assessment of the Potential Soil Erosion and Flood Hazard Zones in Ekiti State, Southwestern Nigeria Using Integrated RUSLE and HAND Models." *Catena* 194: 104725.

Pal, S. C., and R. Chakrabortty. 2019. "Simulating the Impact of Climate Change on Soil Erosion in Sub-Tropical Monsoon Dominated Watershed Based on RUSLE, SCS Runoff and MIROC5 Climatic Model." *Advances in Space Research* 64, no. 2: 352–377. https://doi.org/10.1016/j.asr.2019.04.033.

Panagos, P., P. Borrelli, F. Matthews, et al. 2022. "Global Rainfall Erosivity Projections for 2050 and 2070." *Journal of Hydrology* 610: 127865. https://doi.org/10.1016/j.jhydrol.2022.127865.

Panagos, P., P. Borrelli, and K. Meusburger. 2015. "A New European Slope Length and Steepness Factor (LS-Factor) for Modeling Soil Erosion by Water." *Geosciences* 5, no. 2: 117–126. https://doi.org/10.3390/geosciences5020117.

Panagos, P., P. Borrelli, K. Meusburger, et al. 2017. "Global Rainfall Erosivity Assessment Based on High-Temporal Resolution Rainfall Records." *Scientific Reports* 7, no. 1: 4175. https://doi.org/10.1038/s41598-017-04282-8.

Panagos, P., P. Borrelli, J. Poesen, et al. 2015. "The New Assessment of Soil Loss by Water Erosion in Europe." *Environmental Science & Policy* 54: 438–447.

Panagos, P., F. Matthews, E. Patault, et al. 2024. "Understanding the Cost of Soil Erosion: An Assessment of the Sediment Removal Costs From the Reservoirs of the European Union." *Journal of Cleaner Production* 434: 140183.

Patro, E. R., C. De Michele, G. Granata, and C. Biagini. 2022. "Assessment of Current Reservoir Sedimentation Rate and Storage Capacity Loss: An Italian Overview." *Journal of Environmental Management* 320: 115826.

Pieri, C. J. 2012. *Fertility of Soils: A Future for Farming in the West African Savannah (Vol. 10). Springer Science & Business Media*.

Pillai, B. R. K., and S. Giraud. 2014. "Dam Rehabilitation and Improvement Project (DRIP): 270 Dams to be Rehabilitated." In First National Dam Safety Conference, Chennai, India.

Qin, W., Q. Guo, W. Cao, et al. 2018. "A New RUSLE Slope Length Factor and Its Application to Soil Erosion Assessment in a Loess Plateau Watershed." *Soil and Tillage Research* 182: 10–24. https://doi.org/10.1016/j.still.2018.04.004.

Raj, R., M. Saharia, and S. Chakma. 2023. "Mapping Soil Erodibility Over India." *Catena* 230: 107271. https://doi.org/10.1016/j.catena.2023.107271.

Raj, R., M. Saharia, and S. Chakma. 2024. "Geospatial Modeling and Mapping of Soil Erosion in India." *Catena* 240: 107996.

Raj, R., M. Saharia, S. Chakma, and A. Rafieinasab. 2022. "Mapping Rainfall Erosivity Over India Using Multiple Precipitation Datasets." *Catena* 214: 106256. https://doi.org/10.1016/J.CATENA.2022.106256.

Renard, K. G. 1997. *Predicting Soil Erosion by Water: A Guide to Conservation Planning With the Revised Universal Soil Loss Equation (RUSLE)*. US Department of Agriculture, Agricultural Research Service.

Romshoo, S. A., S. Altaf, I. Rashid, and R. A. Dar. 2018. "Climatic, Geomorphic and Anthropogenic Drivers of the 2014 Extreme Flooding in the Jhelum Basin of Kashmir, India." *Geomatics, Natural Hazards and Risk* 9, no. 1: 224–248.

Romshoo, S. A., S. A. Bhat, and I. Rashid. 2012. "Geoinformatics for Assessing the Morphometric Control on Hydrological Response at Watershed Scale in the Upper Indus Basin." *Journal of Earth System Science* 121: 659–686. https://doi.org/10.1007/s12040-012-0192-8.

Romshoo, S. A., and I. Rashid. 2014. "Assessing the Impacts of Changing Land Cover and Climate on Hokersar Wetland in Indian Himalayas." *Arabian Journal of Geosciences* 7, no. 1: 143–160. https://doi.org/10.1007/s12517-012-0761-9.

Salhi, A., S. Benabdelouahab, and E. Heggy. 2025. "Soil Erosion Susceptibility Maps and Raster Dataset for the Hydrological Basins of North Africa." *Scientific Data* 12, no. 1: 65.

Sarkar, S., and R. Maity. 2024. "Unveiling Climate Change-Induced Temperature-Based Hotspots Across India Through Multimodel Future Analysis From CMIP6." *International Journal of Climatology* 44, no. 2: 627–646.

Sharma, S. K., R. K. Sinha, T. I. Eldho, and H. M. Patel. 2023. "Individual and Combined Impacts of Land Use/Cover and Climate Change on Water Balance Components of a Tropical River Basin." *Environmental Modeling & Assessment* 29, no. 1: 67.

Shojaeezadeh, S. A., M. Al-Wardy, M. R. Nikoo, et al. 2024. "Soil Erosion in the United States: Present and Future (2020–2050)." *Catena* 242: 108074.

Shrestha, B., M. S. Babel, S. Maskey, et al. 2013. "Impact of Climate Change on Sediment Yield in the Mekong River Basin: A Case Study of the Nam Ou Basin, Lao PDR." *Hydrology and Earth System Sciences* 17, no. 1: 1–20.

Siswanto, S. Y., and F. Francés. 2019. "How Land Use/Land Cover Changes Can Affect Water, Flooding and Sedimentation in a Tropical Watershed: A Case Study Using Distributed Modeling in the Upper Citarum Watershed, Indonesia." *Environmental Earth Sciences* 78, no. 17: 550. https://doi.org/10.1007/s12665-019-8561-0.

Solomon, S. D. 2007. *Contribution of Working Group I to the Fourth Assessment Report of the Intergovernmental Panel on Climate Change 2007*. Cambridge University Press.

Stagl, J., E. Mayr, H. Koch, F. F. Hattermann, and S. Huang. 2014. *Effects of Climate Change on the Hydrological Cycle in Central and Eastern Europe*, 31–43. Springer. https://doi.org/10.1007/978-94-007-7960-0_3.

Stryker, J., B. Wemple, and A. Bomblies. 2018. "Modeling the Impacts of Changing Climatic Extremes on Streamflow and Sediment Yield in a Northeastern US Watershed." *Journal of Hydrology: Regional Studies* 17: 83–94. https://doi.org/10.1016/j.ejrh.2018.04.003.

Tabari, H. 2020. "Author Correction: Climate Change Impact on Flood and Extreme Precipitation Increases With Water Availability." *Scientific Reports* 10, no. 1: 16969. https://doi.org/10.1038/s41598-020-74038-4.

Tao, W., J. Wu, and Q. Wang. 2017. "Mathematical Model of Sediment and Solute Transport Along Slope Land in Different Rainfall Pattern Conditions." *Scientific Reports* 7, no. 1: 44082. https://doi.org/10.1038/srep44082.

Tetzlaff, D., J. Seibert, and C. Soulsby. 2009. "Inter-Catchment Comparison to Assess the Influence of Topography and Soils on Catchment Transit Times in a Geomorphic Province; the Cairngorm Mountains, Scotland." *Hydrological Processes* 23, no. 13: 1874–1886.

Tiwari, H., S. P. Rai, D. Kumar, and N. Sharma. 2016. "Rainfall Erosivity Factor for India Using Modified Fourier Index." *Journal of Applied Water Engineering and Research* 4, no. 2: 83–91. https://doi.org/10.1080/23249676.2015.1064038.

Tsegaye, L., and R. Bharti. 2021. "Soil Erosion and Sediment Yield Assessment Using RUSLE and GIS-Based Approach in Anjeb Watershed, Northwest Ethiopia." *SN Applied Sciences* 3, no. 5: 582. https://doi.org/10.1007/s42452-021-04564-x.

United Nations. 2015. *Transforming Our World: The 2030 Agenda for Sustainable Development*. United Nations General Assembly, A/RES/70/1. https://sdgs.un.org/2030agenda.

Williams, J. R. 1975. "Sediment Routing for Agricultural Watersheds." *Journal of the American Water Resources Association* 11, no. 5: 965–974. https://doi.org/10.1111/j.1752-1688.1975.tb01817.x.

10991085, 2025, 9, Downloaded from https://onlinelibrary.wiley.com/doi/10.1002/hyp.70262 by INDIAN INSTITUTE OF TECHNOLOGY (NON -EAL), Wiley Online Library on [21/09/2025]. See the Terms and Conditions (https://onlinelibrary.wiley.com/terms-and-conditions) on Wiley Online Library for rules of use; OA articles are governed by the applicable Creative Commons License

Wischmeier, W. H., and D. D. Smith. 1958. "Rainfall Energy and Its Relationship to Soil Loss." *Transactions of the American Geophysical Union* 39, no. 2: 285. https://doi.org/10.1029/TR039i002p00285.

Wu, S., X. Zhou, J. Reyns, D. Yamazaki, J. Yin, and X. Li. 2024. "Climate Change and Urban Sprawl: Unveiling the Escalating Flood Risks in River Deltas With a Deep Dive Into the GBM River Delta." *Science of the Total Environment* 947: 174703.

Zeghmar, A., E. Mokhtari, and N. Marouf. 2024. "A Machine Learning Approach for RUSLE-Based Soil Erosion Modeling in Beni Haroun Dam Watershed, Northeast Algeria." *Earth Science Informatics* 17: 2921–2936. https://doi.org/10.1007/s12145-024-01305-7.

Zhang, L., Z. Nan, Y. Xu, and S. Li. 2016. "Hydrological Impacts of Land Use Change and Climate Variability in the Headwater Region of the Heihe River Basin, Northwest China." *PLoS One* 11, no. 6: e0158394. https://doi.org/10.1371/journal.pone.0158394.

Supporting Information

Additional supporting information can be found online in the Supporting Information section. **Figure S1:** Comparison of IMD precipitation and bias corrected data for the catchment. **Figure S2:** Clay ratio of Jhelum catchment. **Figure S3:** Modified clay ratio of the Jhelum catchment. **Figure S4:** CLOM (critical level of organic matter) of the Jhelum catchment. **Figure S5:** Percentage importance of different RUSLE parameters for PSL in Jhelum catchment. **Figure S6:** Rainfall ersosivity of Jehlum Catchment under SSP 245 for 2030 (a), 2040 (b), 2050 (c), 2060 (d), 2070 (e), 2080 (f), 2090 (g). **Figure S7:** Rainfall ersosivity of Jehlum Catchment under SSP 585 for 2030 (a), 2040 (b), 2050 (c), 2060 (d), 2070 (e), 2080 (f), 2090 (g). **Figure S8:** Map showing the soil erosion severity map for 2050 (a, c) and 2090 (b, d) under SSP 245 and SSP 585, respectively. **Figure S9:** Map showing the soil erosion severity map for 2020 highlighting severe erosion classes. **Figure S10:** Map showing the soil erosion severity map for 2030 under SSP 245 highlighting severe erosion classes. **Figure S11:** Map showing the soil erosion severity map for 2030 under SSP 585 highlighting severe erosion classes. **Figure S12:** Map showing the soil erosion severity map for 2050 under SSP 245 highlighting severe erosion classes. **Figure S13:** Map showing the soil erosion severity map for 2050 under SSP 585 highlighting severe erosion classes. **Figure S14:** Map showing the soil erosion severity map for 2090 under SSP 245 highlighting severe erosion classes. **Figure S15:** Map showing the soil erosion severity map for 2090 under SSP 585 highlighting severe erosion classes.

10991085, 2025, 9, Downloaded from https://onlinelibrary.wiley.com/doi/10.1002/hyp.70262 by INDIAN INSTITUTE OF TECHNOLOGY (NON -EAL), Wiley Online Library on [21/09/2025]. See the Terms and Conditions (https://onlinelibrary.wiley.com/terms-and-conditions) on Wiley Online Library for rules of use; OA articles are governed by the applicable Creative Commons License